creative commons
COMMONS DEED

저작자표시-비영리-변경금지 2.0 대한민국

이용자는 아래의 조건을 따르는 경우에 한하여 자유롭게

- 이 저작물을 복제, 배포, 전송, 전시, 공연 및 방송할 수 있습니다.

다음과 같은 조건을 따라야 합니다:

저작자표시. 귀하는 원저작자를 표시하여야 합니다.

비영리. 귀하는 이 저작물을 영리 목적으로 이용할 수 없습니다.

변경금지. 귀하는 이 저작물을 개작, 변형 또는 가공할 수 없습니다.

- 귀하는, 이 저작물의 재이용이나 배포의 경우, 이 저작물에 적용된 이용허락조건을 명확하게 나타내어야 합니다.
- 저작권자로부터 별도의 허가를 받으면 이러한 조건들은 적용되지 않습니다.

저작권법에 따른 이용자의 권리는 위의 내용에 의하여 영향을 받지 않습니다.

이것은 이용허락규약(Legal Code)을 이해하기 쉽게 요약한 것입니다.

Disclaimer

dCollection

이학박사 학위논문

Investigation on surface tension of nanoscale water

나노스케일 물의 표면장력 연구

2015년 8월

서울대학교 대학원

물리·천문학부

권 소 영

Investigation on surface tension of nanoscale water

나노스케일 물의 표면장력 연구

指導教授 諸元鎬

이 論文**을** 理學博士學位論文**으로** 提出**함**

2015年 **5** 月

서울大學校 大學院

物理·天文學部

權 素 瑩

權素瑩**의** 理學博士 學位論文**을** 認准**함**

2015年 **6** 月

委 員 長	박 건 식	印
副委員長	제 원 호	印
委 員	홍 승 훈	印
委 員	이 탁 희	印
委 員	곽 호 영	印

Investigation on surface tension of nanoscale water

by

Soyoung Kwon, M.S.

Dissertation

Presented to the Faculty of the Graduate School of

Seoul National University

in Partial Fulfillment

of the Requirements

for the Degree of

Doctor of Philosophy

Seoul National University

August 2015

Abstract

Investigation on surface tension of nanoscale water

Soyoung Kwon
Department of Physics and Astronomy
The Graduate School
Seoul National University

Surface tension plays an important role in nanoscale vapor-liquid phase transition such as condensation, evaporation of nano water meniscus or bubble. The measured and theoretical values due to the formation of it have been disagreed and it was been debated whether the surface tension defined in macroscopic scale is applied the same in nanoscale. However surface tension remain large unknown and imperatively need to be better understood. The capillary rise method is the oldest and most typical way to determine surface tension among several methods of surface tension measurements. We demonstrated a hybrid force measurement system to obtain the capillary force directly so that we could investigate surface tension in nanoscale.

The hybrid system of a quartz tuning fork (QTF)-based, amplitude-modulation atomic force microscope (AM-AFM) and a microelectromechanical system (MEMS) measures simultaneously the dynamic and static forces for nanoconfined water bridge formed between hydrophilic surfaces. This system formed a stable water bridge at a certain distance and obtained the absolute

capillary force besides dynamic properties of the water meniscus. Moreover, the MEMS force sensor provides the additional force information, verifies the AFM measurement, allows accessibility of multiple driving frequencies, and expresses the stress or strain of the confined nanoscale water column. Stress and strain measurements revealed that the nanoconfined water meniscus has the Young's modulus comparable to that of soft rubber or soft tissues and the low loss tangent value close to the solid-like behavior.

We calculated the capillary force on the basis of Young-Laplace equation and compared the analyzed values with the experimental findings. This numerical evaluation of Young-Laplace equation enables the surface tension in nanoscale to be investigated closely. Therefore, we found that the surface tension value of water meniscus in nanoscale significantly decreases less than 20 % of the one in bulk water. This observations may resolve the existing discrepancies between experiments and theories associated with liquid-vapor transition effects in nanoconfined water and allow a contribution to the applications such as self-assembly of bio-molecules and effecient design of nanomaterials.

Keywords : Nanoscale water, Surface tension, Capillary force, Microelectromechanical system, Atomic force microscope

Student number : 2010-30114

Contents

List of Figures

Chapter 1

Introduction

Liquid-vapor phase transition of nanoconfined water cluster and vapor bubble formation can be observed in various physical systems. The experimental investigations and theoretical predictions were found to be significantly different and still remained unresolved controversy. Diverse measurements developed show quantitative but qualitative agreements and clarification of the above discrepancy can be achieved by modifying surface tension value [1, 2]. For water at 25°C, tensile strength for a vapor bubble formation expected from the theory is over 1,000 atm [3, 4] while the actual value of experiment is 277 atm [5]. Energy barrier for liquid nanometric meniscus to turn into vapor and vice versa shows substantially smaller value in experiments [6, 7] to theory [8]. A cluster model for a bubble formation suggests smaller surface tension value rather than bulk value treated as macroscopic and this approach can be applied to nanometric meniscus as well. However, the theory of the curvature dependence of

surface tension was established [9] and has been studied experimentally, there are still questions regarding the surface tension at the interface in small system in contrast to bulk [10–13]. Young-Laplace equation relevant to the shape of the surface describes the capillary pressure difference sustained across the interface due to the phenomenon of surface tension or wall tension which is fundamentally important in presence of capillary surfaces [14]. Water molecules on the surface of a meniscus have fewer neighbors to bond while those inside of liquid have possible connection to all directions. Thus, the former water molecules are bounded more weakly than the latter and make the surface curved with internal pressure. The theory of the curvature dependence of surface tension was well formulated over a half-century ago [9] and experimental support is established in cavities ever since [14]. Further surface tension study still required when meniscus of water in nanoscale shares similar characteristics in bulk liquid. Physical properties of many materials and interfaces including capillary water meniscus at nanoscale are different comparing with their values at macroscale for several reasons, such as high surface-to-volume ratios and different physical mechanisms [15]. Thus, the effect of the surface tension which is responsible for curvature of meniscus seems to dominate over the influence relevant to volume in nanoscale phenomena. The curvature dependence of surface tension has been of interest, however, yet to be established experimentally well and there are still questions regarding the surface tension at the interface in small system in contrast to bulk. There are various methods of surface tension measurements such as drop weight method, maximum bulk pressure method, analyzing shape

of the hanging liquid drop or gas bubble [16, 17]. Among these, a capillary rise method is the oldest and typical way to determine the surface tension in macroscopic scale. A research been done for the microcapillaries experiment assuming the surface tension value as a macroscopic one since the method was developed for measuring radii of microcapillaries and the viscosity of liquids in them not the surface tension itself. We demonstrated a hybrid system of a quartz tuning fork (QTF)-based, amplitude-modulation (AM) AFM and a microelectromechanical system (MEMS) to investigate the surface tension by the stable formation of water meniscus. Several have focused on the formation of capillary bridges between two surfaces and both the viscoelastic forces and hydrodynamics forces that arise [18]. Since the surface forces apparatus (SFA) was introduced in 1976 [20], study of the interfacial materials submerged in a liquid medium was activated by investigating the interaction forces. Similar technique of the surface force balance (SFB) has also been useful tool to reveal nanoscopic properties and nanotribology different from the bulk fluids, such as increment of effective viscosity in the mediums [28]. Tip-based study of interaction forces with mapping and imaging of the surface contributed the improvement of the nanotribological understandings with dynamic force microscopy (DFM) [29]. Study of nanoscale surfaces using SFA/B, atomic force microscopy (AFM), scanning tunneling microscopy (STM) typically requires either an UHV or liquid environment to overcome unwilling effects of capillary force between the tip and the sample, which is critical in mapping and imaging. However, the capillary force of naturally confined interfacial water in a nanometer gap in ambient condi-

tions rather gives a critical clue to understand the bio-molecular behavior with the AFM system [30]. On the contrary to other approaches, we have performed our experiments in ambient conditions and formed a nano water bridge, a feature researchers often try to avoid in their experimental setups, to study the capillary force in between two surfaces. Over the last several years, we have worked on pioneering the AM-AFM as a reliable method for capillary condensation and viscoelastic measurements [31,34,35]. Unlike traditional approaches, which use the compliant cantilever, we have investigated the use of the quartz tuning fork which provides many useful characteristics to formation of stable water meniscus. The focus of this dissertation is the hybrid MEMS-AFM system for investigating surface tension with capillary condensed nanometric water meniscus. In Chapter 2, a quartz tuning fork based atomic force microscopy and surface micro-machined MEMS force sensor to study capillary condensed water nanomeniscus is described in detail. In Chapter 3, the hybrid MEMS-AFM system which employs a QTF based AFM to measure the dynamic response of water meniscus while MEMS force sensor simultaneously and directly measures such a static forces as the capillary, adhesion, and hydrodynamic force. In Chapter 4, on the assumption that the curvature of meniscus is maintained during approach and retraction procedures in the experiments, the numerical evaluation of Young-Laplace equation enables the surface tension in nanoscale to be investigated closely. Hence, we theoretically calculate the capillary force on the basis of Young-Laplace equation with a constant curvature hypothesis and compare the analyzed values with the experimental findings. In this work, we

quantified the surface tension in nanoscale by measurement of the total capillary force resulting from the water nano-meniscus in combination with theoretical calculation.

Bibliography

[1] R. Zhang, A. Khalizov, L. Wang, M. Hu, and W. Xu, Chem. Rev. **112**, 1957 (2012).

[2] P. E. Wagner, and R. Strey, J. Chem. Phys. **80**, 5266 (1984).

[3] J. C. Fisher, J. Appl. Phys. **19**, 1062 (1948).

[4] H. N. V. Temperley, Proc. phys. Soc. **59**, 199 (1947).

[5] L. J. Briggs, J. Appl. Phys. **21**, 721 (1950).

[6] W. Bak, B. Sung, J. Kim, S. Kim, B. Kim, and W. Jhe, Appl. Phys. Lett.**106**, 013102 (2015).

[7] B. Sung, J. Kim, C. Stambaugh, S. Chang, and W. Jhe, Appl. Phys. Lett. **103**, 213107 (2013).

[8] Y. Men, X. Zhang, and W. Wang, J. Chem. Phys. **131**, 184702 (2009).

[9] R. C. Tolman, J. Chem. Phys. **16**, 758 (1948).

[10] T. Mitsui, M. K. Rose, E. Fomin, D. F. Ogletree, and M. Salmeron, Sience **297**, 1850 (2002).

[11] K. B. Jinesh, J. W. M. Frenken, Phys. Rev, Lett.**96**, 166103 (2006).

[12] J. Gao, R. Szoszkiewicz, U. Landman, and E. Riedo, Phys. Rev. B **75**, 115415 (2007).

[13] Y. Zhu, and S. Granick, Phys. Rev. Lett.**87**, 096104 (2001).

[14] F. M. Orr, L. E. Scriven, J. Fluid Mech.**67**, 723 (1975).

[15] D. S. Choi, M. S. Jhon, H. Eyring, J. Chem. Phys. **53**, 2608 (1970).

[16] S. Kwon, C. Stambaugh, B. Kim, S. An, and W. Jhe, Nanoscale **6**, 5754 (2014).

[17] N. V. Churayev, V. D. Sobolev, and Z. M. Zorin, Special Discussions of the Faraday Society **1**, 213 (1970).

[18] A. W. Adamson, and A. P. Gast, *Physical chemistry of surfaces, 6 edi* (Wiley, 1997).

[19] C. D. Willett, M. J. Adams, S. A. Johnson, and J. P. K. Seville, Langmuir **16**, 9396 (2000).

[20] J. N. Israelachvili and G. E. Adams, Nature **262**, 774 (1976).

[21] J. Klein and E. Kumacheva, Science **269**, 816 (1995).

[22] F. J. Giessibl, Rev. Mod. Phys.**75**, 949 (2003).

[23] R. Garcia, R. Magerle, and R. Perez, Nature Mater. **6**, 405 (2007).

[24] M. Lee, B. Sung, N. Hashemi, and W. Jhe, Faraday Discuss. **141**, 415 (2009).

[25] M. Lee and W. Jhe, Phys. Rev. Lett. **97**, 1 (2006).

[26] B. Kim, S. Kwon, H. Mun, S. An, and W. Jhe, Sci. Rep. **4**, 6499 (2014).

Chapter 2

Hybrid MEMS-AFM system

The forces that arise from the presence of liquids play an important role in many systems. To investigate such interactions we have developed and tested a measurement platform that combines the viscoelastic sensitivity of a home-built quartz tuning force based atomic force microscope with the force measuring capability of a micro-electromechanical force sensor.

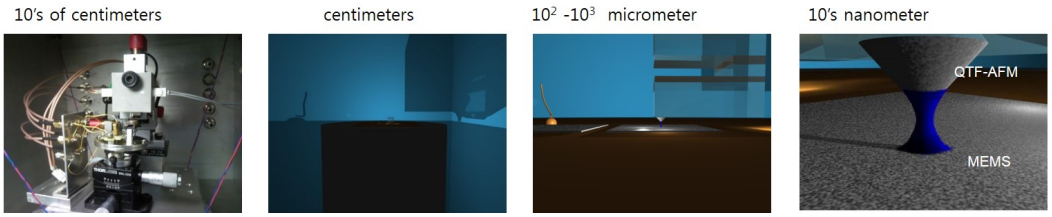

Figure 2.1: Hybrid MEMS-AFM and the nanometric water meniscus formed between the tip and the surface in ambient condition. From the scale of 10's of centimeters to 1's of nanometer. The leftmost picture is the hybrid MEMS-AFM setup inside of inner chamber surrounded by bigger humidity controlled outer chamber and the rightmost image presents the nanometric water meniscus confined schematically.

2.1 Quartz tunning fork (QTF)-based Atomic force microscopy (AFM)

Over the last several years, we have worked on pioneering the amplitude modulation (AM) QTF-AFM as a reliable method for studying viscoelasticity [1–3] unlike traditional approaches, which use the compliant cantilever beam. The QTF provides many useful characteristics, such as reasonably high quality factor ($\sim$ 5000), simple electrical detection, high stiffness ($10^3 \sim 10^4$ N/m) [4, 5] . Thus it is well suited for measurements of the nanometric water meniscus in ambient condition due to no susceptibility of the pull-in effects resulting from van der Waals interaction that generally occurs in conventional cantilever-based AFM system [6,7]. We use Quartz tip fabricated by a commercial laser puller (P-2000, Sutter Instruments Co.) to produce tips that are more rigid yet still have radii below 100nm and the AFM tip oscillates perpendicular to the substrate.

Assuming small oscillations a linear oscillator model which describes the motion of the QTF can be applied as,

$$m\ddot{x} + b\dot{x} + kx = F\cos\omega t + F_{\text{int}}, \tag{2.1}$$

here m is the effective mass of the probe, b is the damping coefficient, k the spring constant of QTF, ω the driving frequency, F the amplitude of the driving force, and F_{int} the interaction force which is the quantity of interest.

An interacted elasticity (k_{int}) and viscosity (b_{int}) can be written as follows,

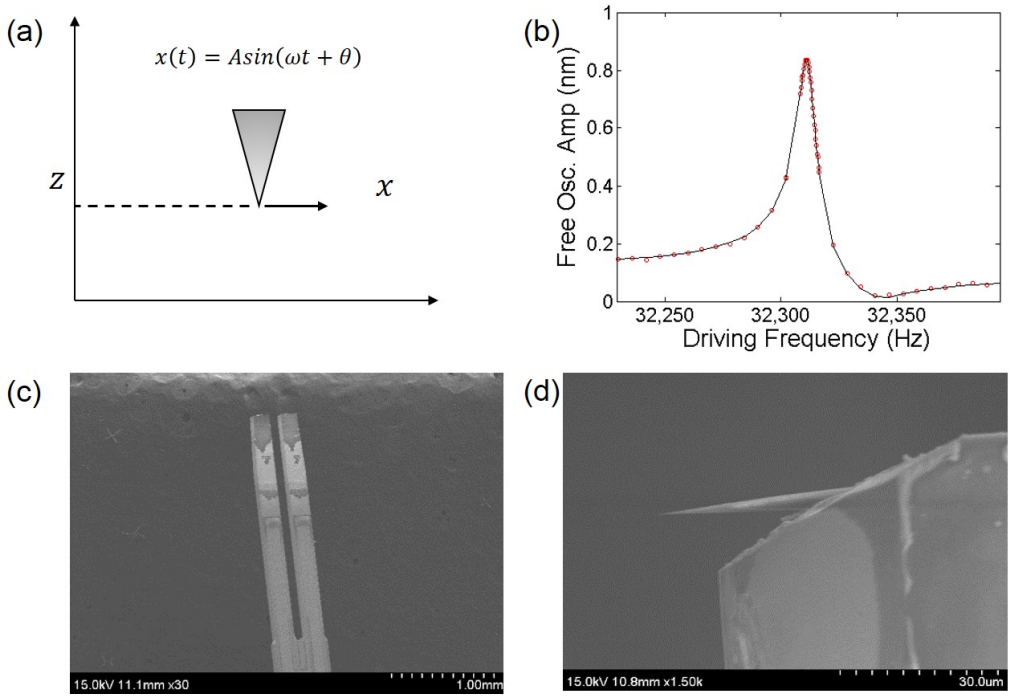

Figure 2.2: QTF-AFM system (a) QTF oscillates for simple harmonic motion. (b) Output oscillating amplitude of QTF resonator. (c) Piezoelectric device of QTF combines with the pulled nanopipette. The tapping- and shear-mode operation of the QTF-based AFM. (d) The tapping tip oscillates vertically to the top of the MEMS surface, while the shearing tip vibrates parallel to the surface.

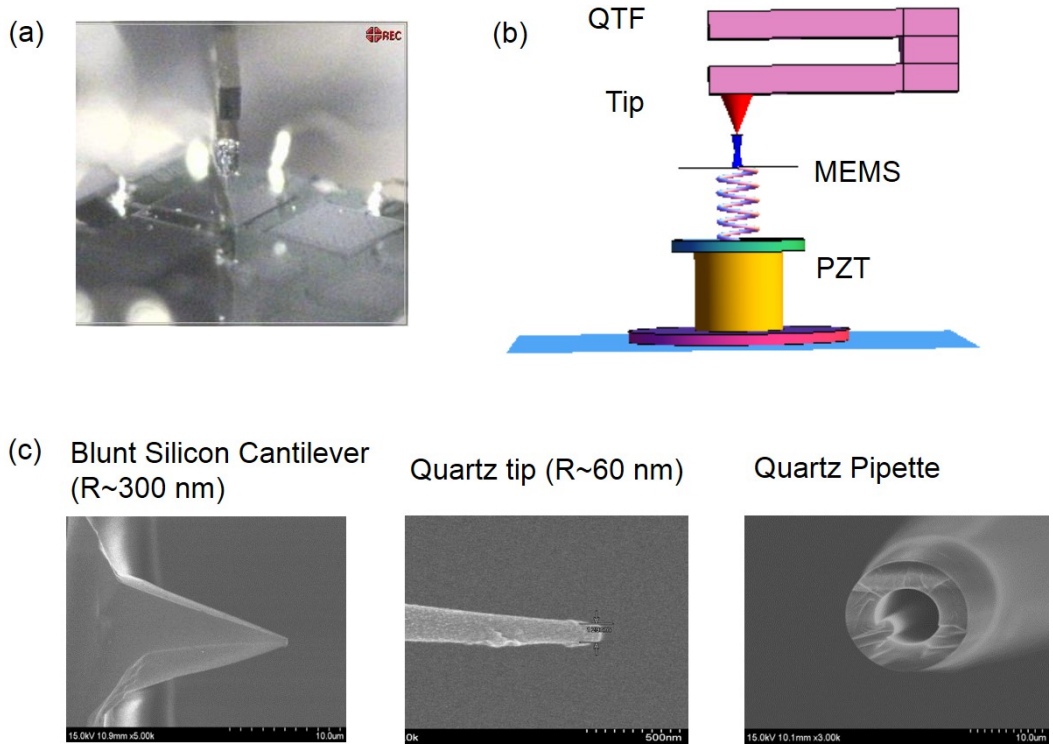

Figure 2.3: Experimental setup of nanometric force measurement system. (a) An alignment of the tapping mode experiment. A quartz tip is attached on the bottom of the QTF and aligned right above the center of a movable MEMS plate. (b) schematic image the system. QTF probe places above the MEMS force sensor attached on the PZT and the water meniscus confined in between the QTF probe and the MEMS substrate when they get closer than certain distance apart. (c) SEM images of different tips such as silicon cantilever tip, fabricated quartz tip and pipette.

$$k_{\text{int}} = \frac{F}{A(z)}\sin\theta(z) + m\omega^2 - k, \tag{2.2}$$

$$b_{\text{int}} = \frac{F}{A(z)\omega}\cos\theta(z) - b, \tag{2.3}$$

here A is an amplitude of the QTF output signal. While the QTF sensor provides the information of the viscoelastic properties of the confined nanoscale water meniscus [8–11], it is limited to provide the absolute force on position, which is possible to measure with MEMS force sensor.

2.2 Microelectromachanical system (MEMS) force sensor

2.2.1 Surface micro-machining of z-axis force sensor

The force sensor used in this setup (FIg. 2.4) is a micro-electromechanical sensor and actuator referred to as MEMS, fabricated by MEMSCAP Co. using the polyMUMPS of surface micromachining process [12]. We want a device that can be used to measure force in the z-axis and the most basic force sensor is a spring using Hooke's Law $F = kx$. We only need to measure the displacement and multiply by the spring to determine the force as shown in Fig. 2.5. For the nanoscale water to form and pull on it, a flat surface that is attached to the spring, is needed. The forces and changes in position are on the nanoscale so a sensitive device and detection technique are required, a well chosen spring constant as well.

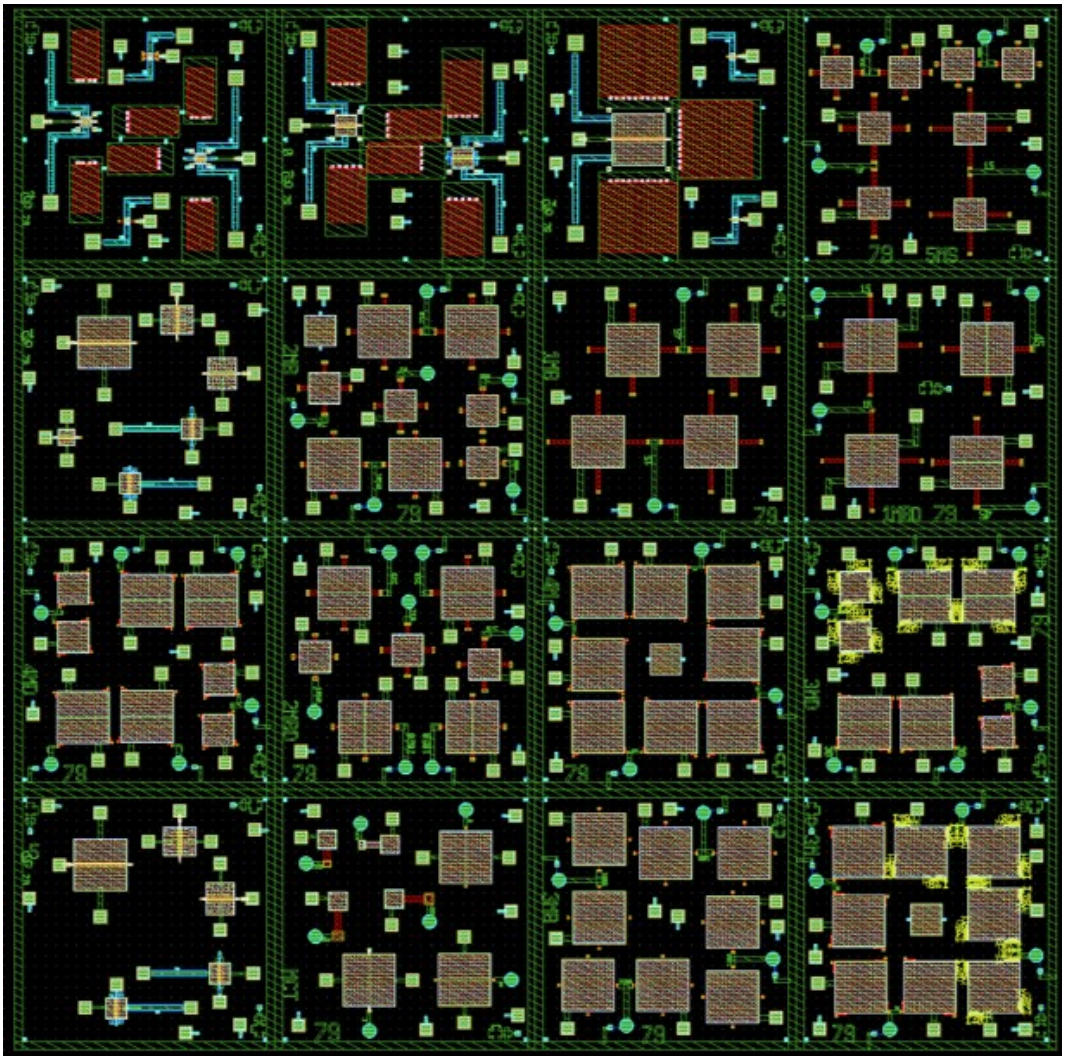

Figure 2.4: The design for fabrication. We utilized the commercial foundry MEMSCAP where the polyMUMPS process is used for surface micro-machining.

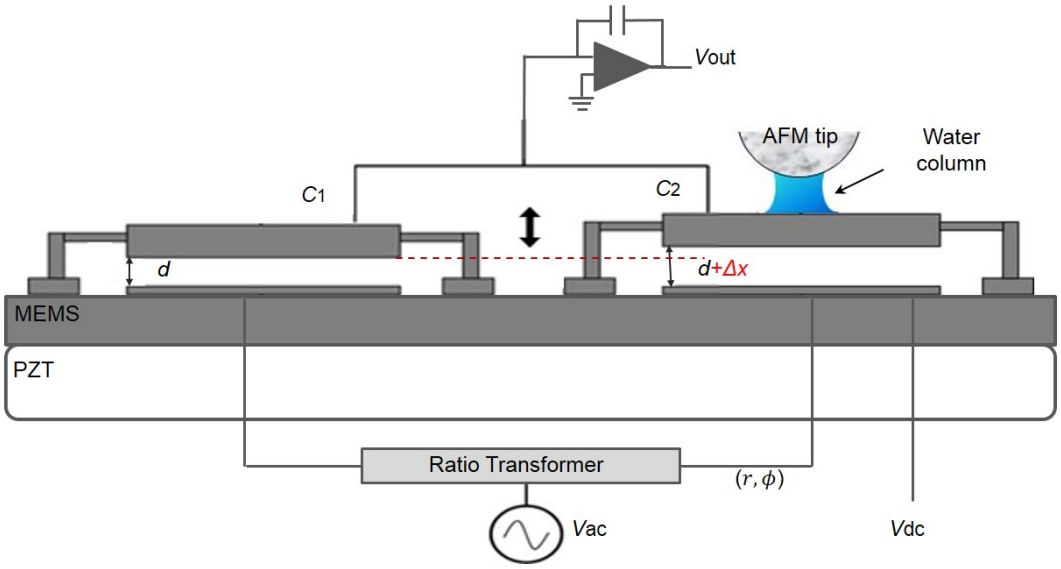

Figure 2.5: Schematic of the detection method of nanometric water column formed between the MEMS and the QTF. A differential capacitance measurement technique is used to optimize the detection of the plate's displacement. The displacement of the plate (Δx) gives information of the interaction forces.

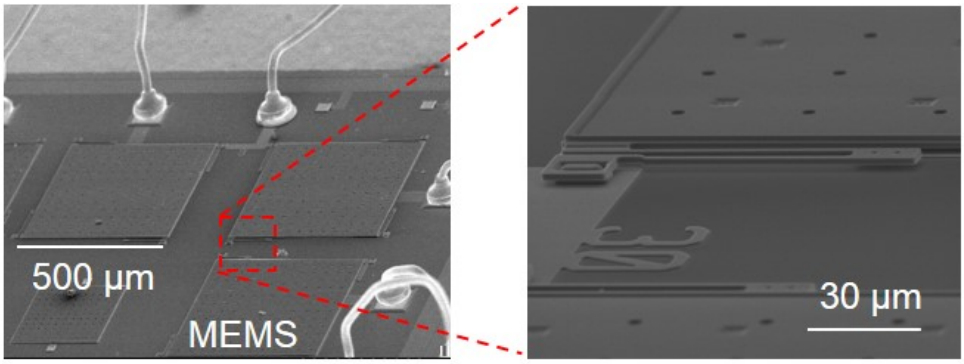

Figure 2.6: SEM images of the fabricated MEMS. Each device is composed of an electrically isolated ground layer and another layer of poly-silicon (500 μm $\times$ 500 μm), which image is captured by scanning electron microscope (SEM).

The requirement of sensitivity on the nanoscale means a MEMS/NEMS type of device is a good choice and the most sensitive measurement techniques involve measuring changes in capacitance with the requirement of out of plane movement (z-axis) the method of surface-micromachining is the best choice. Surface micromachining is based on the deposition and etching of different structural layers on top of a substrate [13, 14] and the devices we fabricated are shown in Fig. 2.6. This is in opposition to bulk micromachining which defines structures by selectively etching inside a substrate. Whereas surface micromachining creates structures on top of a substrate, bulk micromachining produces structures inside a substrate.

2.2.2 Shear MEMS device works along x- and y-axes

In addition to the tensile MEMS device works in z-axis, we designed a shear mode MEMS device fabricated with silicon-on-insulator micromachining SOI-MUMPs process(Fig.2.7). It makes the shear force measurement possible by applying strain in x-axis as well as y-axis. Two additional PZT movable in shear directions(x- and y-axes on a plane) is stacked up above the tube PZT movable in z-axis in order to give a strain in all directions. The nanometic water bridge forms when the AFM tip approaches to the MEMS surface with z-axis PZT and the interaction force is investigated with the strain in shear directions. While the water bridge holds stably by a feedback program, one can elongate or slide the water along with the movement applied in x- or y- axis with the shear PZT as shown in Fig. 2.8 and Fig. 2.9.

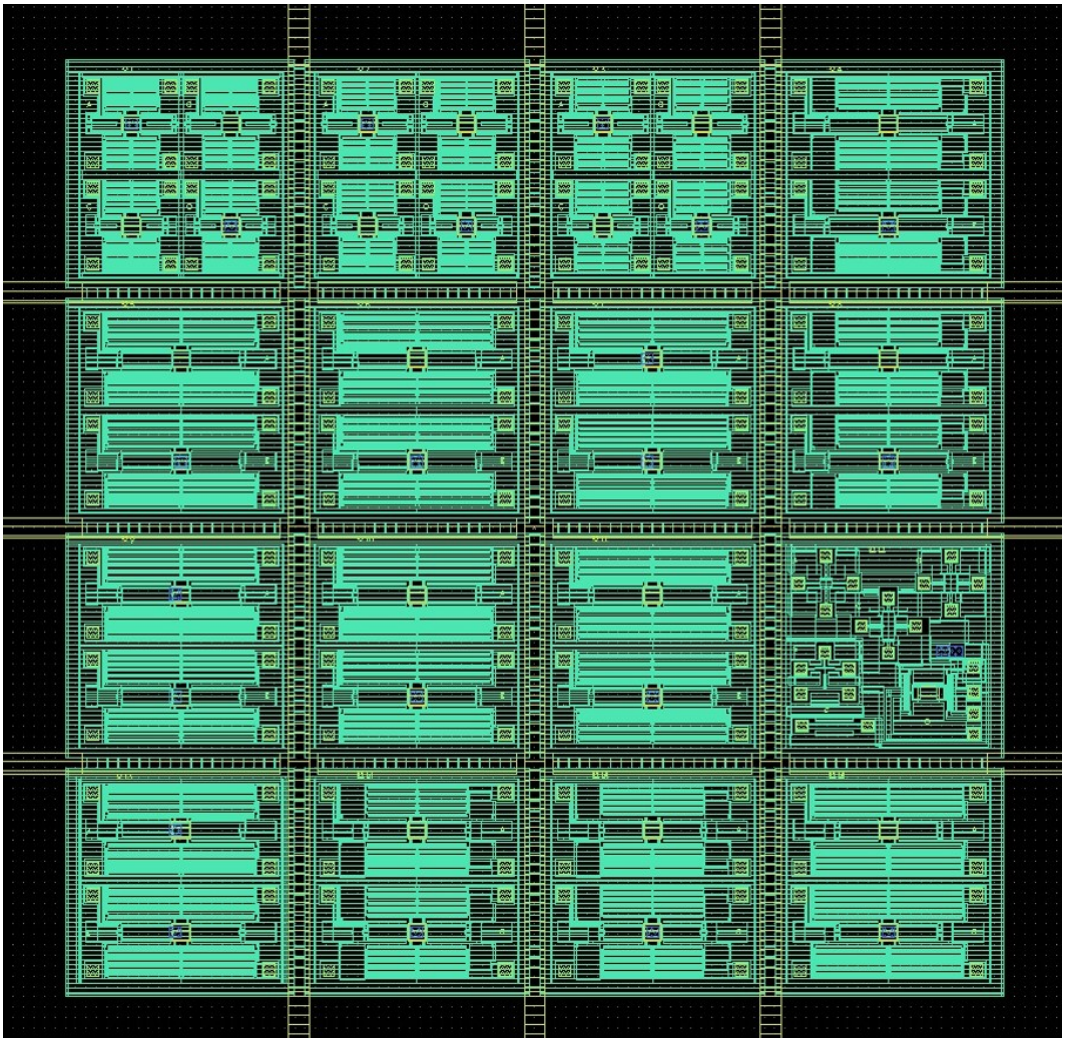

Figure 2.7: The design for fabrication of the shear MEMS device. We utilized the commercial foundry MEMSCAP where the SOIMUMPs process is used for surface micro-machining.

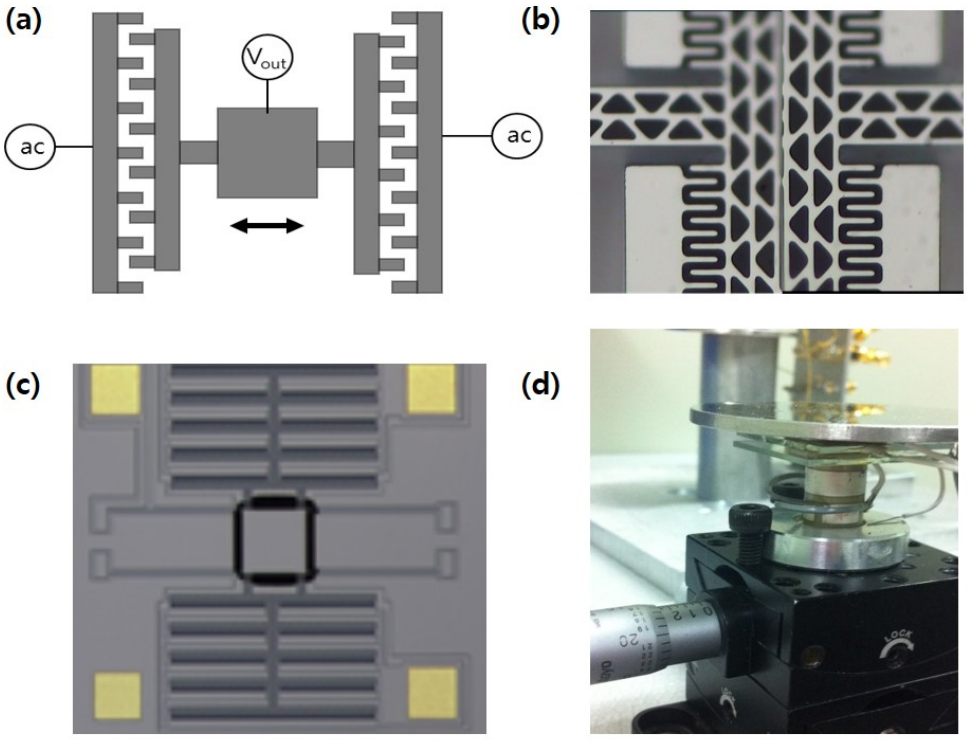

Figure 2.8: Shear MEMS device works along x-axis. (a) Schematic image of the shear MEMS device. (b) Comb part which contributes to measurement of interaction force. (c) Microscope image of the device and electrode gold pads which will be wire-bondng to make the package for the hybrid MEMS-AFM system. (d) Stacked PZTs. A tube PZT sensitively movable in z-axis and plane plate PZTs in x- and y- axes. Every surfaces were coated with gold (Hitachi E-1010, Ion sputter) and glued with conductive epoxy to help with elecrical contact.

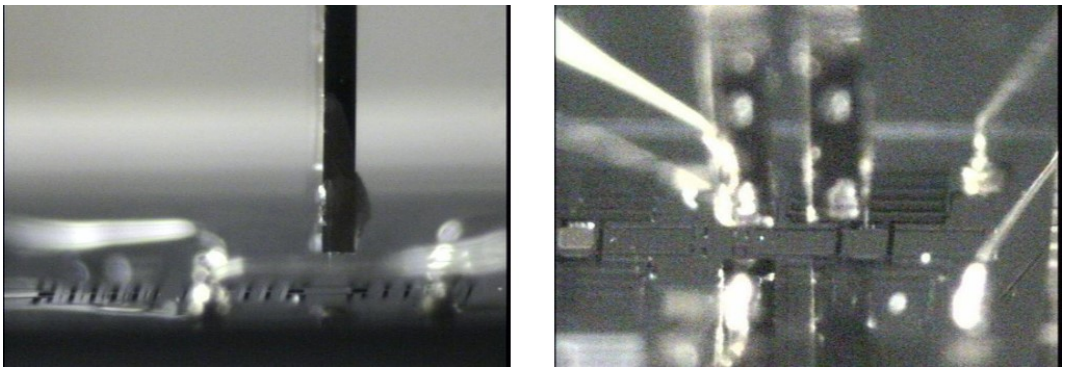

Figure 2.9: Shear stress measurement. (a) Front of chamber view, that is y-axis. (b) Left side of chamber view, x-axis. Signal of MEMS device occurs when the center plate moves with water meniscus in x- or y- directions

2.2.3 MEMS in hybrid system

The use of MEMS provides several nice features including the ability to easily fabricate duplicates of each structure, and only minimal design modification is needed to produce devices of varying sensitivity. The well-known force sensing system of MEMS is the interfacial force microscope (IFM) which utilizes a torsional type device with an attached tip to probe the interactions with a surface. This type of device works in a closed-loop feedback mode where the gap is fixed by varying direct current (DC) voltage. Cheneler et al. proposed a device design to use MEMS to monitor viscoelastic properties of thin films with low frequency [15]. Apart from overall methodology, our MEMS device is more focused on the interaction forces of nanoscale liquid meniscus, though our design was originally designed for use of a magnetometer and this approach is suited to examine the low frequency properties as well. Figure 2 shows the demonstrated MEMS force sensor. Each device is composed of an electrically

isolated ground layer and another layer of poly-silicon (500 μm $\times$ 500 μm), which image is captured by scanning electron microscope (SEM) in Fig. 2(a). The response of the MEMS sensor is performed with external stimuli. Electrostatic force exerts on the two plates by applying a DC voltage (Fig. 2(b)). The plate displacement (Δx) gives information of the interaction forces. The movable top plates are suspended with a distance of 2 µm above the ground layer by four poly-silicon springs connected to each electrode. Figure 2(c) shows a schematic of the devices. The capacitance between the ground plate and the movable plate of the MEMS is written as $C = \epsilon_0 A/d$ (A is the area the two plates overlap, ϵ_0 is the permittivity of free space and d is the gap between two plates). Note that the change of d is used to detect the interaction forces with movement of the plate. The dimension of the springs determines the spring constant and thus the resonant frequency of the device and force sensitivity. The detection scheme is a differential capacitance measurement technique used to optimize the detection of the plate's displacement [14, 16]. Single pair of the plates is used as the fixed reference capacitance (C_1) and the movable test capacitance (C_2). An alternative current (AC) voltage (V_{ac}) is applied to the bottom electrodes of the capacitors. The phase difference between the two AC signals is 180° and the relative amplitude is adjusted using a ratio transformer so that the output signal is zero which depends on the difference of the capacitors is as follows,

$$V_{\text{out}} = V_{\text{ac}} \frac{(C_1 - C_2)}{\beta}, \tag{2.4}$$

here β is the charge to voltage factor from the charge sensitive amplifier (Amptek 500) and V_{ac} is the applied AC voltage. The output signal of the MEMS is obtained from the variation of the donating capacitance (C_2). The displacement (Δx) of one plate is determined by solving Eq. (4) assuming the geometry is determined from the device design,

$$\Delta x = \frac{V_{\mathrm{out}} d^2}{V_{\mathrm{out}} d - \beta A \epsilon_0 V_{\mathrm{ac}}}, \tag{2.5}$$

here A is a surface area of the MEMS plate. When the nanometric water meniscus spontaneously forms, it applies an attractive force on the top plate of the MEMS device. This causes the plate to rise up and change the distance between the test capacitor. Equation 6 states that this change in the test capacitance leads to a change in x, which can be measured and converted to the actual force applied by the water column onto the movable MEMS plates.

$$F_{\mathrm{electrostatic}} = \frac{\epsilon_0 A {V_{\mathrm{dc}}}^2}{2(d - \Delta x)^2}, \tag{2.6}$$

$$F_{\mathrm{MEMS}} = k_{\mathrm{MEMS}} x(V_{\mathrm{out}}), \tag{2.7}$$

here V_{dc} is an applied DC voltage and Δx is the change in position measured from d. Since the electrostatic force is well known, and the response signal is approximately linear for small changes in x, the output signal (V_{out}) can be converted to MEMS detection force (F_{MEMS}), assuming the spring constant of the device is known.

2.3 Hybrid MEMS-AFM system

Non-contact AFM has been well suited for studying the interaction forces with boundary conditions such as Van der Waals force, electrostatic force but not the capillary force which has no exact boundary conditions. Contact AFM can measure the capillary force except the dynamic properties like damping coefficient and energy dissipation. The enhanced hybrid system, however, can provide both the dynamic properties using the QTF-AFM with improvement of previous non-contact AFM and the static properties by directly measuring the force using the MEMS sensor. Especially, the MEMS force sensor provides the additional force information, verifies the QTF measurement, allows accessibility of multiple driving frequencies, and expresses the stress or strain of the confined nanoscale water column.

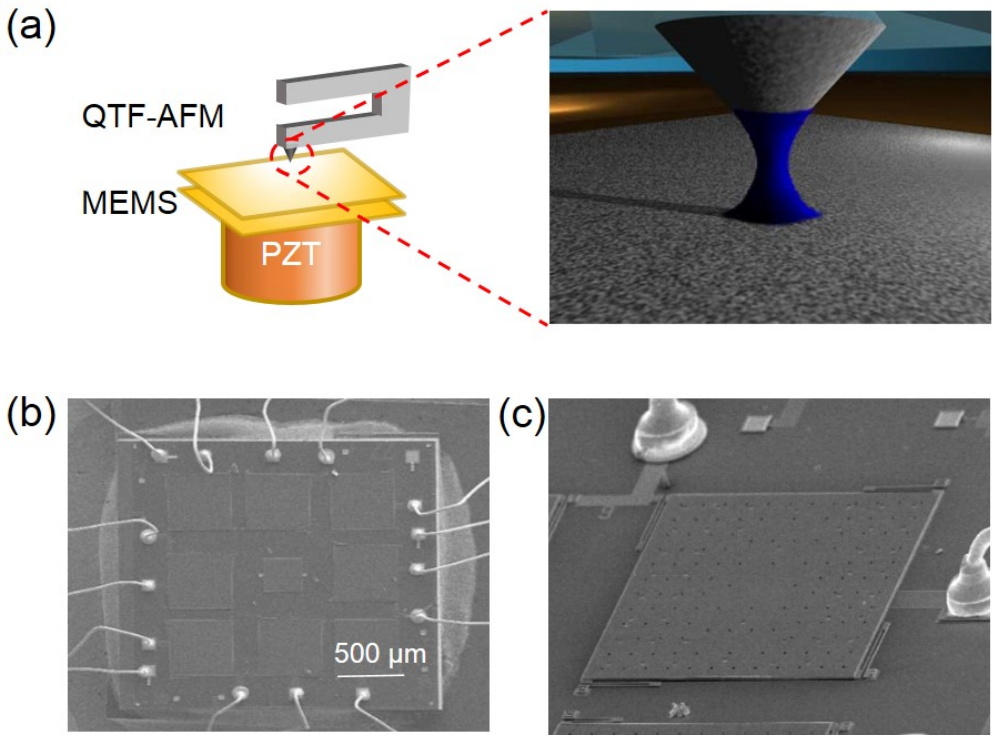

Figure 2.10: Hybrid MEMS-AFM and the nanometric water meniscus formed between the tip and the surface in ambient condition. (a) The QTF approaches the MEMS force sensor which is mounted onto a PZT tube and the concave water meniscus forms. (b) The SEM image of surface micro-machining of z-axis force sensor which has been used in the tapping-mode experiments. (c) Each device has four springs in the corners of a square with different spring constant designed.

Bibliography

[1] F. J. Giessible, Rev. Mod. Phys. **75**, 949 (2003).

[2] M. Lee and W. Jhe, Phys. Rev. Lett **97**, 1 (2006).

[3] M. Lee, J. Jahng, K. Kim, and W. Jhe, Appl. Phys. Lett. **91**, 023117 (2007).

[4] M. Lee, B. Sung, N. Hashemi, and W. Jhe, Faraday Discuss. **141**, 415 (2009).

[5] K. Karrai, and I. Tiemann, Phys. Rev. B **62**, 13174 (2000).

[6] F. J. Giessibl, Appl. Phys. Lett. **73** 3956 (1998).

[7] B. Kim, S. Kwon, H. Mun, S. An, and W. Jhe, Sci. Rep. **4**, 6499 (2014).

[8] S. An, B. Sung, H. Noh, C. Stambaugh, S. Kwon, K. Lee, B. Kim, Q. Kim, and W. Jhe, Nano-Micro Lett. **6**, 70 (2014).

[9] B. Kim, Q. Kim, S. Kwon, K. Lee, M. Lee, and W. Jhe, Phys. Rev. Lett. **111**, 246102 (2013).

[10] H. J. Butt, and M. Kappl, Adv. Colloid Interface Sci. **146**, 48 (2009).

[11] B. Kim, S. Kwon, G. Moon, and W. Jhe, Phys. Rev. E **91**, 032307 (2015).

[12] K. Ninios, T. Hong, T. Manabe, C. Hotta, S. N. Herringer, M. M. Turnbull, C. P. Landee, Y. Takano, and H. Chan, Phys. Rev. Lett. **108**, 097201 (2012).

[13] N. Maluf, and K. Williams, *An introduction to microelectromechanical systems engineering 2nd edi.* (Artech House, 2004).

[14] G. T. A. Kovacs, *Micromachined transducers sourcebook* (WCB/McGraw-Hill, 1998).

[15] D. Cheneler, M. Ward, M. Adams, and Z. Zhang, Sens. Actuator B-Chem. **130**, 701 (2008).

[16] M. Bao, and H. Yang, Sens. Actuator A **136**, 3 (2007).

Chapter 3

Dynamic and Static force measurement using Hybrid MEMS-AFM

Water in nano-confined space is important to incredibly wide range of everyday phenomena as well as many areas in physical science and nanotechnology with its ubiquitous presence on the surfaces under ambient condition. Condensed water as a nanometric meniscus under ambient conditions and their intriguing behavior has physical importance in wide areas of nanoscale science and technology. This has received a great interest with relevant fields such as nanotribology, nanolithography, nanoparticle self-assembly. The properties of nanometric capillary water meniscus and influence of its surface tension remain large unknown parameters and imperatively need to be better understood. We

present a theoretical and experimental approaches for surface tension of the nanometric confined water by using information of liquid-mediated interaction capillary force measured by a hybrid system of atomic force microscope and microelectromechanical system.

3.1 Introduction

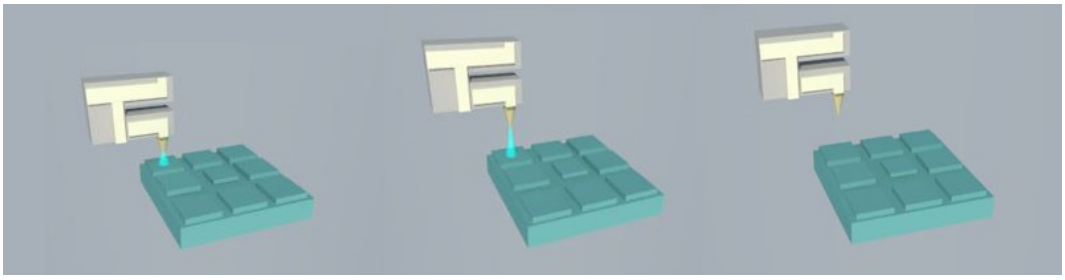

Figure 3.1: Capillary force obtained by the hybrid MEMS-AFM system. The MEMS plate is retracted and the water meniscus is elongated until it finally breaks free and the capillary foce obtained during this approach/ retract procedure.

The interaction force between surfaces has a major effect on the behavior of the materials, such as nanoparticles, proteins, various bio-molecules, and so on [1–3]. The phenomenon of stiction influenced by interaction forces impacts the repetitive use of the devices based on the micro/nanoscale materials [4]. Although there have been several studies to discover the origin of the interaction forces including Van der Waals, Casimir, Electrostatic, and hydrodynamic forces for the purpose of energy conservation with various systems [5–7], it is difficult to solve and still challenging issues to investigate the force effected molecular

behaviors. In particular, the role of liquids at the interface is more important to understand the vital phenomena in the field of nano-biosience [8, 9]. Among these works, Willett et al. have focused on the formation of capillary bridges between two surfaces with the viscoelastic and hydrodynamics forces [10]. Since the surface forces apparatus (SFA) was introduced in 1976 [11], study of the interfacial materials submerged in a liquid medium was activated by investigating the interaction forces. Similar technique of the surface force balance (SFB) has also been useful tool to reveal nanoscopic properties and nanotribology different from the bulk fluids, such as increment of effective viscosity in the mediums [12]. Tip-based study of interaction forces with mapping and imaging of the surface contributed the improvement of the nanotribological understandings with dynamic force microscopy (DFM) [13].

Study of nanoscale surfaces using SFA/B, atomic force microscopy (AFM), scanning tunneling microscopy (STM) typically requires either an UHV or liquid environment to overcome unwilling effects of capillary force between the tip and the sample, which is critical in mapping and imaging. However, the capillary force of naturally confined interfacial water in a nanometer gap in ambient conditions rather gives a critical clue to understand the bio-molecular behavior with the AFM system [14, 15].

In this chapter, we present the hybrid MEMS-AFM system for investigation of the interacted dynamic and static force resulting from surfaces and liquids. This system employs a QTF-based AFM to measure the dynamic response of a nanoscale column of water, while a MEMS force sensor simultane-

ously measures physical quantities.

3.2 Dynamic and Static force measurement

The basic experiment perform is as follows and figure 3.2 shows the experiment process of the approach and retraction curve which is generally used to determine the mechanical properties of nanoscale materials. First the MEMS plate approaches to the QTF probe by incremental moving extending PZT located below the MEMS device (step I in Fig.3.2). Then the capillary condensed nanometric water column suddenly forms between two surfaces within a few nanometers, while the monitoring signals of QTF and MEMS change dramatically (step II in Fig. 3.2). This causes the top plate to rise up and change the distance between the movable capacitor. And the MEMS device approaches closer to the tip in the presence of the water column to investigate the properties of the materials (step III in Fig. 3.2). Finally, the PZT is subsequently retracted and the water meniscus is stretched (step IV in Fig. 3.2) until it finally breaks free.

The contact point is determined as the position where the effective elasticity(k_{int}) turns into positive showing an abrupt increase in its value as shown in Fig. 3.3(a).

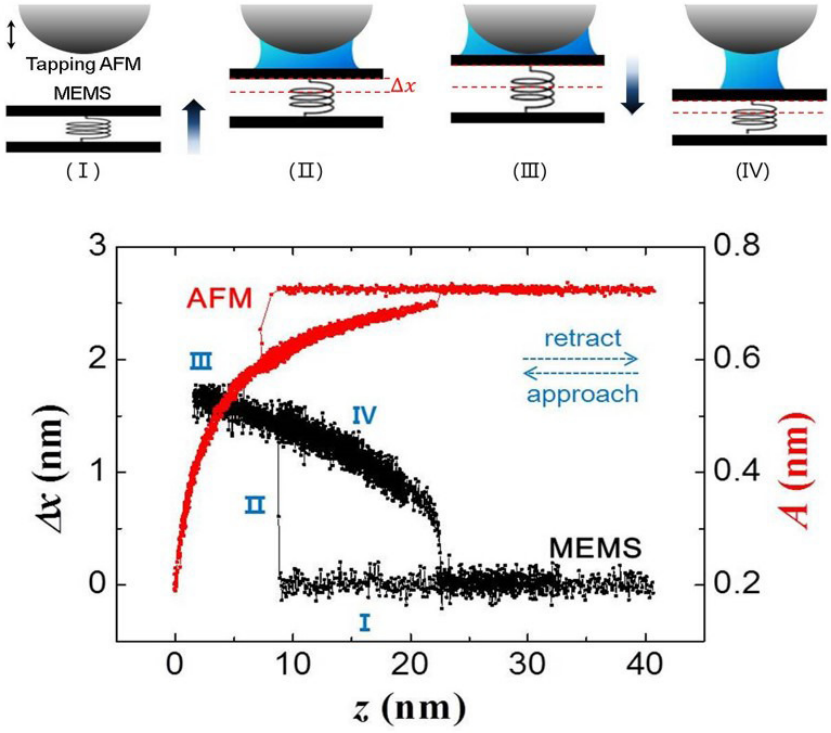

Figure 3.2: Experiment procedure. The plots are the simultaneous responses of the AFM and MEMS including the formation of the during the approach/retraction cycle: (I) Approach the MEMS substrate close to the QTF probe, (II) instant movement of the top plate in the MEMS device due to the formation of the water column by capillary condensation, (III) incremental change in MEMS plate's displacement as it approaches closer, (IV) retraction and rupture of the water meniscus.

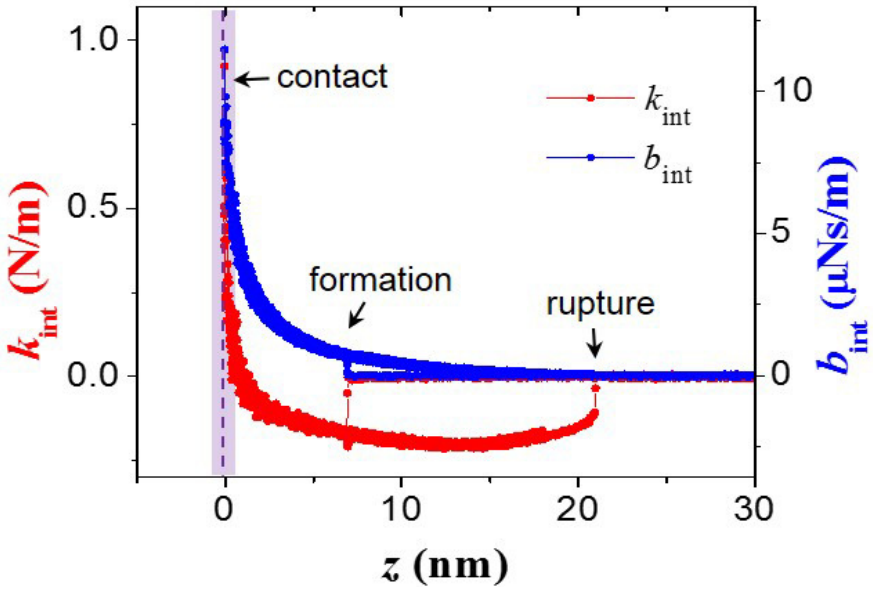

Figure 3.3: Experimental result from hybrid MEMS-AFM and determination of contact point: The effective elasticity (k_{int}) and damping coefficient (b_{int}) of the nanoscale water cluster obtained by the QTF-based AFM and the contact point.

3.3 Capillary force of nanoscale water cluster

Figure 3.4 shows the experiment results obtained by the hybrid MEMS-AFM. The amplitude and phase values of QTF-AFM are converted into the force(F_{AFM}) and compared with MEMS results which is important part in this work to confirm the exact values of interaction forces.

$$F_{\mathrm{AFM}} = \int_{z_r}^{z} dz[-k_{\mathrm{int}}] + F_0, \tag{3.1}$$

here z_r is rupture distance, F_0 is a constant of integration, and k is force gradient in small oscillation. Nevertheless, the force gradient with the amplitude phase values obtained by the AFM itself cannot be simply integrated to the force with a constant of integration unknown due to its discontinuous behavior associated with formation or rupture of the water cluster. While other interaction forces such as Van der Waals, electrostatic force have a boundary condition that is zero at infinity, the capillary force has no such a boundary condition with the discontinuity in amplitude and phase results. Simultaneous measurement presented here provides crucial information for non-contact AFM to obtain the capillary foce besides dynamic characteristics of nanoconfined water cluster. Henceforward, quantitative results in detail will be discussed so that the AFM study could take this advantage for obtaining the absolute capillary force in nanoscale.

Figure 3.4 shows the calculated forces curves of the QTF and the MEMS, which are matched each other and this indicates that the two approaches strongly concur with each other in this view. Having the ability to directly measure the

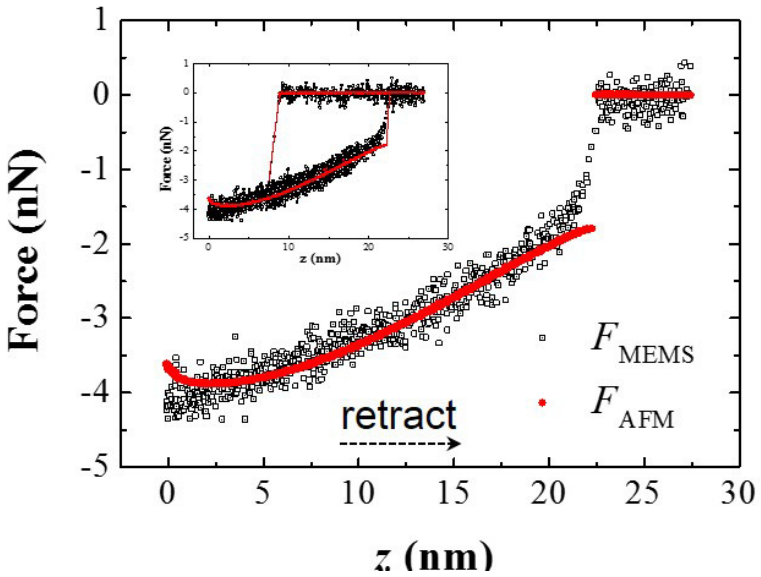

Figure 3.4: Capillary force obtained by the hybrid MEMS-AFM system. The calculated capillary forces for the QTF-based AFM as well as the directly measured forces by the MEMS force sensor in the entire approach and retraction procedure. Here, the integration constant F_0 for F_{AFM} is set to -1.8 nN (red curve) showing the best fit with the F_{MEMS}. The result shows that the two approaches can work together significantly well.

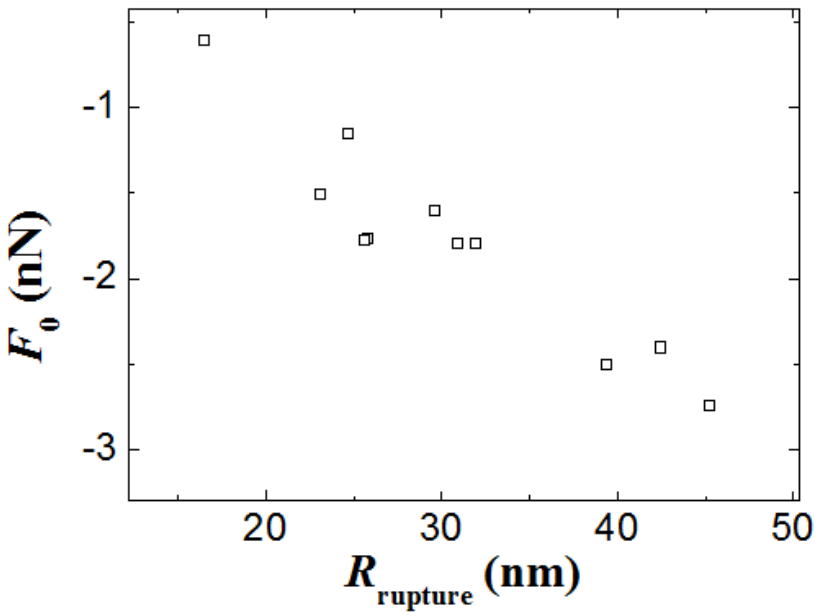

Figure 3.5: The integral constant F_0 which is crucial to convert the force gradient value by AFM to the absolute capillary force in entire range. The value F_0 seems to have a linear dependency along with rupture distance of water meniscus.

elasticity, viscosity and force of the water column provides many useful features. The first thing is a confirmation of what the quantities is exactly measured by variation of the QTF signal. A better understanding of the nanometric water column and the system capavilities is obtained by simultaneously and directly measuring the absolute force with the MEMS and dynamic properties such as elasticity 'k_{int}' and viscosity 'b_{int}' with the QTF-AFM. Furthermore, the hybrid MEMS-AFM provides conclusive evidence for the reliability of the previous quantitative analysis of the QTF-AFM based on the fact that the interaction force obtained by the QTF-AFM and the MEMS individually is the same as shown in fig. 3.5.

3.4 Viscoelasticity of nanoscale water cluster

We also find that the effective elasticity is positive near the substrate and its value decreases to negative as the water column is elongated while retracting the MEMS plate (Fig. 3.4(a)). The elasticity k appears to be positive in the vicinity of the substrate due to the short-range repulsive hydration force while negative in a region relatively far from the surface where attractive capillary and van der Waals force dominate. And a damping coefficient here is two orders of magnitude greater than the value expected with viscosity of bulk water. Intriguingly the viscosity at about 7 nm where we have done this experiment appears to be different from bulk. Water meniscus formed in a fairly big gap regarding previous distribution that nanometric water with over a couple of

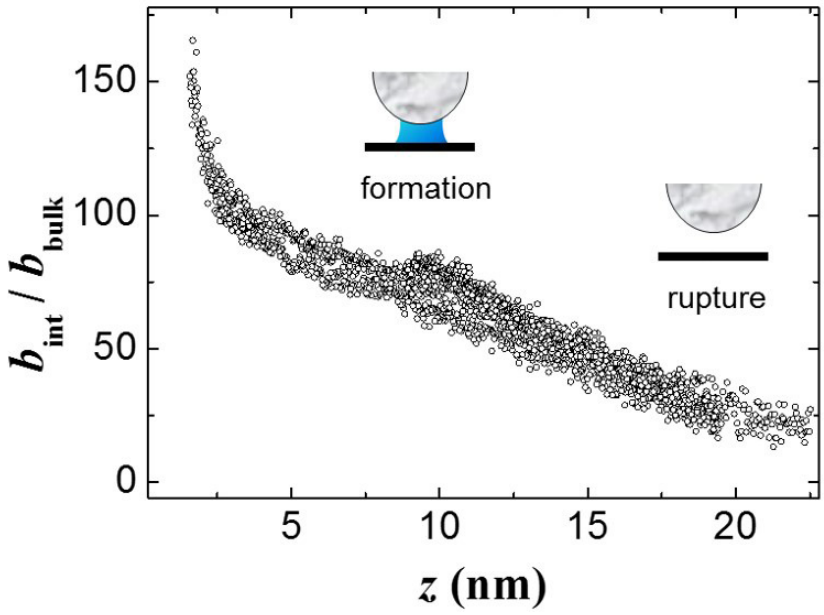

Figure 3.6: The effective viscosity calculated and compared with its bulk value in entire procedure. The viscosity of nanometric water meniscus obtained in typical measurement shows 66 times larger at formation point and 27 times at rupture point.

nano meter gap has an effective viscosity nearly the same as bulk [16, 17]. It is considerd as a result of water meniscus confined in between rather discussed to be thr property of water in nanoscale.

Figure 3.6 shows the effective viscosity of nanoscale water cluster compared to its bulk value. The viscosity measured for the nanoscale water cluster is about 66 times to 27 times larger than the calculated viscosity based on the bulk model at formation and rupture. We found a large increase in the effective viscosity while no significant changes in viscosity of nanoconfined water in aqueous environment reported at a few nanometer. Therefore we can presume

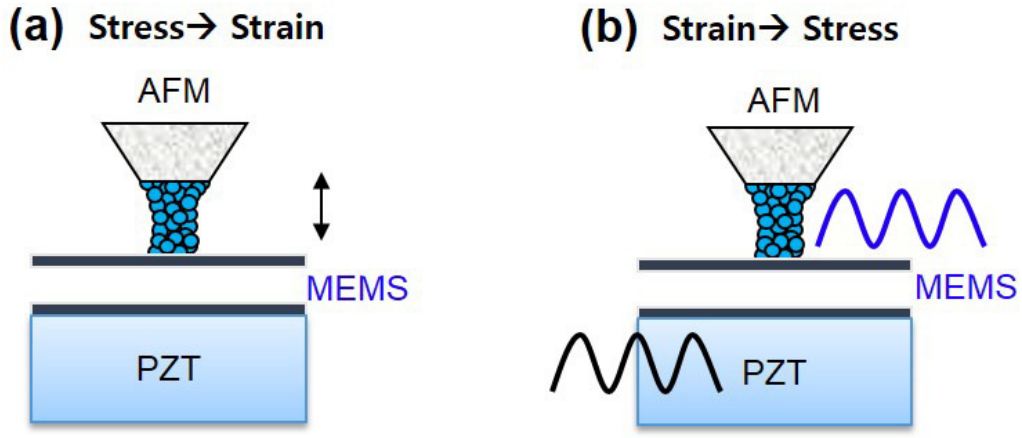

Figure 3.7: Strain-stress measurement. (a) The hybrid system measures the interaction force as stress resulting from strain which applied to the nanometric water meniscus by approaching and retracting the MEMS surfaces to the AFM tip. (b) The system obtain the strain in MEMS device due to the stress applied sinusoidal by oscillating the PZT.

it is affected by the surface tension effect of meniscus rather than an intrinsic viscosity change in water at nanoscale.

A further research of the viscoelasticity in nanometric liquid materials is performed according to the strain and the stress measurement. Hybrid MEMS-AFM system allows us to investigate this different approach besides the interaction force measurement to study nanometric liquid due to the benefits of the direct real time measurement technic.The typical experiments are performed as a stress-strain measurement, that is, interaction force of nanometric water confinement can be obtrained by change in a capacitance (Fig. 3.7 (a)). A sinusoidal tensile strain by stretched or compressed material leads to stress when the nanometric water is confined in between the tip and the substrate within a few nanometers with driving stress ahead of the strain as shown in Fig. 3.7 (b).

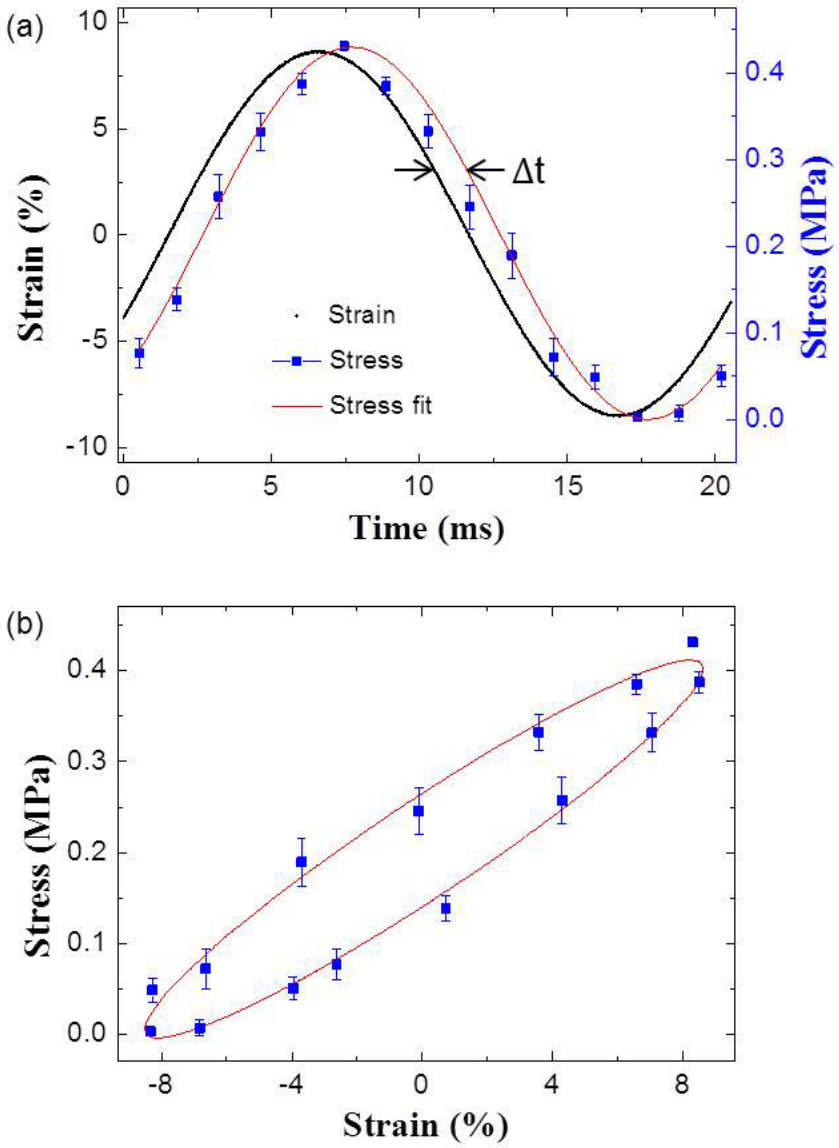

Figure 3.8: Comparison of displacement and force response as strain and stress, respectively. (a) Dynamic response of the nanometric water to sinusoidal load by oscillating PZT at the frequency of 270Hz in time. (b) Load-displacement curve (stress-strain) obtained by the nanometric water showing the dynamical and mechanical hysteresis.

The strain-stress curve makes us obtain young's modulus and effective relaxation time of the nanometric water and provides extended knowledge of nanometric material. When the strain is sinusoidal in time $\epsilon(t) = \epsilon_0 \sin(2\pi\nu t)$, the stress is $\sigma(t) = \sigma_0 \sin(2\pi\nu t - \delta)$ and retarded with the phase angle δ [18]. The effective relaxation time [18] ($\Delta t = \delta/2\pi\nu$) obtained directly from this result is 4.18×10^{-5}s which is similar to that calculated by the static demonstration with AFM results, 3×10^{-6}s (Fig. 3.8(a)). The elliptical Lissajous figure is a consequence of linearly viscoelastic behavior of nanometric water (Fig. 3.8(b)).

Loss tangent is high for liquid-like materials but low for solid-like materials. Even though we oscillate slow as 50Hz the loss tangent is 1.6×10^{-4} and close to solid-like at this frequency while extremly faster oscillation can cause solidity with the picosecond scale relaxation time of water. Young's modulus of nanometric water is 2.5 MPa which is comparable with that of soft rubbers and soft tissues (1-10MPa, $\sim$2.5 for some tissues) [19, 20].

3.5 Conclusion

We demonstrated the hybrid MEMS-AFM scheme to provide both direct and indirect information of the discontinuous as well as continuous forces associated with the water cluster in nanoscale. In particular, the capillary force obtained in entire length besides the dynamic properties in nanosale. The calculated interaction force for the QTF-based AFM and the diretly measured force by MEMS force sensor are in excellent agreement. Furthermore, the result can

provide more information which is crucial for the QTF-based AFM to obtain absolute capillary force of confined water meniscus. We are progressing on the study of qualitative and quantitative analysis for the capillary force in-depth which intensifies the study on the characteristics and behaviors of the confined liquids in such a small systems.

Bibliography

[1] S. Cai and B. Bhushan, Nanotechnology **18**, 465704 (2007).

[2] M. Carrion-Vazquez, H. Li, H. Lu, P. E. Marszalek, A. F. Oberhauser and J. M. Fernandez, Nat. Struct. Mol. Biol. **10**, 738 (2003).

[3] S. Iyer, R. M. Gaikwad, V. Subba-Rao, C. D. Woodworth and Igor Sokolov, Nat. Nanotechnol. **4**, 389 (2009).

[4] M. Urbakh, J. Klafter, D. Gourdon, and J. Israelachvili, Nature **430**, 525 (2004).

[5] J. Israelachvili, *Intermolecular and Surface Forces* (Academic Press, New York, 2011).

[6] A. E. Nel, L. Mdler, D. Velegol, T. Xia, E. M. V. Hoek, P. Somasundaran, F. Klaessig, V. Castranova, and M. Thompson, Nature Mater. **8**, 543 (2009).

[7] A. Frlich, F. Gabel, M. Jasnin, U. Lehnert, D. Oesterhelt, A. M. Stadler, M. Tehei, M. Weik, K. Wood, and G. Zaccai, Faraday Discuss. **141**, 117(2009).

[8] A. E. Nel, L. Mädler, D. Velegol, T. Xia, E. M. V. Hoek, P. Somasundaran, F. Klaessig, V. Castranova and M. Thompson, Nature Mater. **8**, 543 (2009).

[9] A. Frolich, F. Gabel, M. Jasnin, U. Lehnert, D. Oesterhelt, A. M. Stadler, M. Tehei, M. Weik, K. Wood and G. Zaccai, Faraday Discuss. **141**, 117 (2009).

[10] C. D. Willett, M. J. Adams, S. A. Johnson and J. P. K. Seville, Langmuir **16**,9396 (2000).

[11] J. N. Israelachvili and G. E. Adams, Nature **262**, 774 (1976).

[12] J. Klein and E. Kumacheva, Science **297**, 1540 (2002)

[13] F. J. Giessibl, Rev. Mod. Phys. **75**, 949 (2003)

[14] K. B. Jinesh, and J. W. M. Frenken, Phys. Rev. Lett. **96**, 166103 (2006).

[15] R. Garcia, R. Magerle and R. Perez, Nature Mater. **6**, 405 (2007).

[16] S. H. Khan, G. Matei, S. Patil, and P. M. Hoffmann, Phys. Rev. Lett. **105**, 106101 (2010).

[17] Y. Zhu, and S. Granick, Phys. Rev. Lett. **87**, 096104 (2001).

[18] R. S. Lakes, *Viscoelastic Solids* (CRC Press, 1999).

[19] C. T. McKee, J. A. Last, P. Russell, and C. J. Murphy, Tissue Eng. Part B, **17**, 155 (2011).

[20] R. G. Larson, *The Structure and Rheology of Complex Fluids* (New York : Oxford University Press, 1999).

Chapter 4

Investigation on surface tension of nanoscale water

4.1 Introduction

Liquid-vapor phase transition in small system can be observed in various phenomena such as nucleation of nanoconfined water cluster, vapor bubble and liquid droplets [1, 2]. The experimental investigations and theoretical predictions were found to be significantly different and still remained unresolved controversy. Diverse measurements developed show quantitative but qualitative agreements. For water at 25°C, tensile strength for a vapor bubble nucleation expected from the theory is over 1,000 atm [3, 4] while the actual value of experiment is 277 atm [5]. Energy barrier for liquid nanometric meniscus to turn into vapor and vice versa shows substantially smaller value in experiments [6, 7] to theory [8].

Thus, abundant theoretical studies of the curvature dependent surface tension have been developed to clarify the discrepancy [1, 9]. A cluster model for a bubble formation suggests smaller surface tension value rather than bulk value treated as macroscopic and this approach can be applied to nanometric meniscus as well [3,10]. The theory of the curvature dependence of surface tension was well formulated over a half-century ago [9] and experimental support is established in cavities ever since. Further surface tension study still required when meniscus of water in nanoscale shares similar characteristics in bulk liquid. Physical properties of many materials and interfaces including capillary water meniscus at nanoscale are different comparing with their values at macroscale for several reasons, such as high surface-to-volume ratios and different physical mechanisms. Thus, the effect of the surface tension which is responsible for curvature of meniscus seems to dominate over the influence relevant to volume in nanoscale phenomena. Nevertheless, the properties of nanometric capillary water meniscus and influence due to the surface tension remain large unknown parameters and there is an imperative needed to be better understood.

The curvature dependence of surface tension has been of interest, however, yet to be established experimentally well and there are still questions regarding the surface tension at the interface in small system in contrast to bulk [11–14]. Here, we investigate a hybrid system of a quartz tuning fork (QTF)-based, amplitude-modulation atomic force microscope (AM-AFM) and a microelectromechanical system (MEMS) to measure simultaneously the dynamic and static forces for nanoconfined water cluster formed between hy-

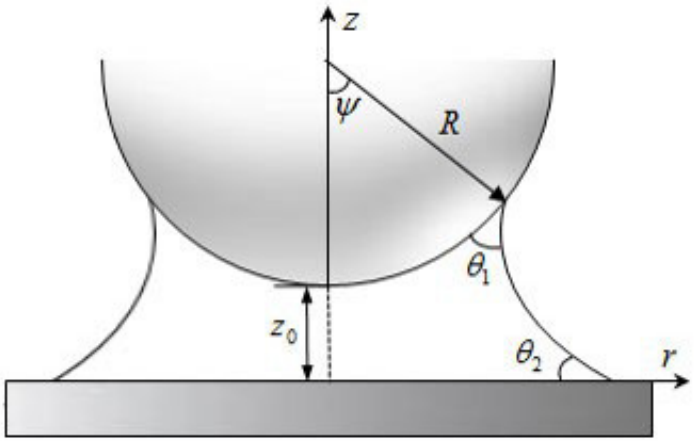

Figure 4.1: A schematic representation of a liquid meniscus formed between a spherical tip and a plane substrate separated by a distance z_0 with a filling angle ψ, the AFM tip radius of curvature R, water contact angles θ_1 and θ_2 of solid surfaces.

drophilic surfaces [15, 16]. The curvature dependent surface tension is obtained in nanoscale by the comparison of the experimentally measured capillary force with the analysed results in relevant to Young-Laplace equation [17]. The capillary force proportional to the surface tension tells us that it decrease to the value less than 0.3 times of macroscopic surface tension in small system which corresponds to what nucleation theories predicts as well [3, 10] .

4.2 Method and modeling of capillary force

4.2.1 Modeling for measured force using capillary force

The total interaction force of the meniscus can be calculated by the sum of the surface tension force and the capillary force as follow [17]. The total capillary

force exerted through the nanometric water meniscus is comprised of three parts: a surface tension force which resides in the meniscus, a capillary pressure force which originates with the meniscus curvature and a buoyancy force related with the wetting. The effect of gravity if negligible, so does the buoyancy force. The surface tension force acting on the spherical probe is

$$F_s = 2\pi R\gamma \sin(\theta_1 + \psi), \tag{4.1}$$

with the filling angle ψ which is related to tip-sample distance z, the AFM tip radius of curvature R, surface tension γ of the interface, the water contact angleθ_1 of solid surface. The theoretical analysis was performed for contact angle θ=0 of the nanometric water bride condensed between hydrophilic surfaces with a small volume. Each filling angle has two solutions. One is the same as physical phenomenon in nature and the other is far away from the fact this solution to be true, that is, water bridge becomes narrow and the force turns weak when the tip gets closer to the surface The force of adhesion due to the capillary pressure can be calculated by

$$F_p = -\pi \frac{\gamma}{r_m} R^2 \sin^2\psi, \tag{4.2}$$

Therefore, the total interaction force of the meniscus can be calculated by the sum of the surface tension force and the capillary pressure force.

$$F_t = F_s + F_p = 2\pi R\gamma \left[\sin\psi \sin(\theta_1 + \psi) - \frac{1}{2r_m} R\sin^2\psi\right], \tag{4.3}$$

Additionally, if we consider the capillary force acting on the plane surface,

it follows in the form

$$F_t(s) = 2\pi x_2 \gamma \left[\sin(\theta_2) - \frac{1}{2r_m} x_2 \right] \tag{4.4}$$

as a sum of the surface tension force

$$F_s(s) = 2\pi x_2 \gamma \sin(\theta_2) \tag{4.5}$$

and the capillary pressure force

$$F_p(s) = -\pi \frac{\gamma}{r_m} {x_2}^2 \tag{4.6}$$

This is exactly true for a plane below or for a spherical surface above that the capillary force can be obtained the same as shown in Fig. 4.2. Figure 4.2 (a) the force obtained by the tip above and (b) for the substrate of MEMS force sensor below. The surface-tension force F_s which caused by contact line of lilquid, vapor and solid and the capillary-pressure force F_p originated by pressure difference between liquid and vapor shows different values but as a sum of these force, the total capillary force F_t calculated with both the tip and the plate are exactly the same as shown in Fig. 4.2 (c).

4.2.2 Solution of Young-Laplace equation

General expression for the principal curvatures of any surface of revolution is,

$$\frac{1}{r_m} = \frac{d^2z/dr^2}{[1 + (dz/dr)^2]^{3/2}} + \frac{dz/dr}{r[1 + (dz/dr)^2]^{1/2}}. \tag{4.7}$$

With dimensionless variables $y = z/R$, $x = r/R$ and the parameter $u = -\sin\epsilon$ and $dy/dx = \tan\epsilon$, where η is the angle mode by the normal to the meniscus

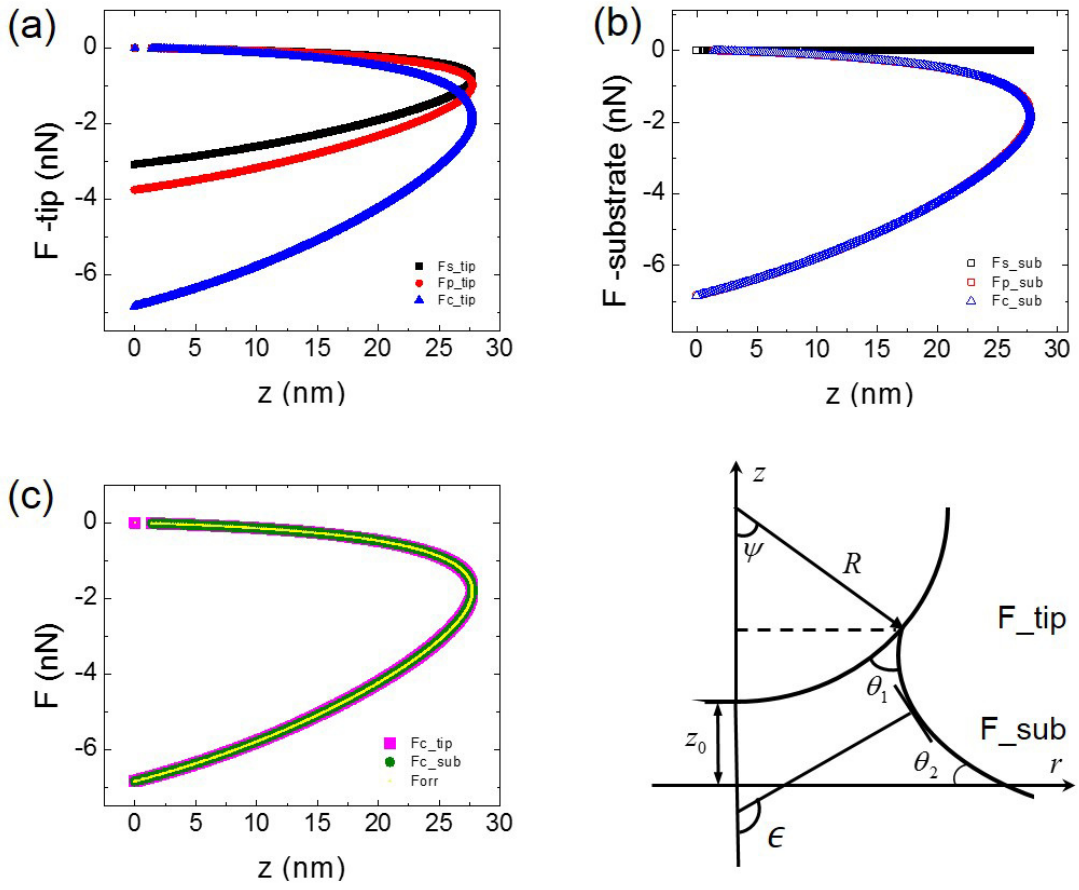

Figure 4.2: The capillary force comparison for a plane or for a spherical substrate. According to the numerical analysis of the capillary force modeling, the force can be caculated with both the tip and the plate and the same result obtained for the total capillary force.

with the vertical axis, the Eq. 4.7 reduces to

$$\frac{R}{r_m} = -\frac{du}{dx} - \frac{u}{x}. \tag{4.8}$$

This differential equation describing the nodoid profile in terms of the function $x(u)$ must be solved as a two-point boundary value problem. The boundary conditions are

$$\begin{aligned} u_2 &= -\sin(\pi - \theta_2), \\ y_2 &= 0, \\ u_1 &= -\sin(\theta_1 + \psi), \\ y_1 &= z_0 + 1 - \cos\psi, \\ x_1 &= \sin\psi, \end{aligned} \tag{4.9}$$

The researting expression for $x(u)$ as the solution of the differential equation is

$$x = -r_m \left[u \mp (u^2 + c)^{1/2} \right] \tag{4.10}$$

where the curvature-dependent parameter c is

$$c \equiv \left(\frac{R}{r_m} \sin\psi \right)^2 - 2\frac{R}{r_m} \sin\psi \sin(\theta_1 + \psi). \tag{4.11}$$

The solution for $y(u)$ is written as

$$y = \frac{r_m}{R} \int_{u_2}^{u} \frac{u du}{(1 - u^2)^{1/2}} \frac{u \mp (u^2 + c)^{1/2}}{\mp (u^2 + c)^{1/2}} \tag{4.12}$$

and by extending the integration to the point of contact (u_1, y_1), we obtain

$$y = \frac{r_m}{R} \left[-\cos\epsilon - \cos\theta_2 - \frac{1}{k}[E(\Phi_2, k) - E(\Phi, k)] + \frac{1 - k^2}{k}[F(\Phi_2, k) - F(\Phi, k)] \right] \tag{4.13}$$

The functions $E(\Phi, k)$ and $F(\Phi, k)$ are elliptic integral of the second and first kind, respectively. The modulus and amplitude are

$$\begin{aligned} k &\equiv \frac{1}{1+c^{1/2}}, \\ \Phi_2 &= \theta_2 - \frac{1}{2}\pi, \\ \Phi &= \frac{1}{2}\pi - \epsilon. \end{aligned} \tag{4.14}$$

4.2.3 Comparison between experimental results and theoretical calculations

The experimental observation described above is now explained by a theoretic model. The configuration of a liquid-vapor interface at rest in an axially symmetric capillary water meniscus is analyzed by the Young-Laplace equation [17]. Note that the tips are sufficiently small to justify the neglect of gravity [15] and the mean curvature of meniscus is nearly uniform. To analyze the interaction force exerted by the capillary condensed water meniscus, either the pressure within the liquid meniscus or the volume of the meniscus is treated as a constant. The shape of meniscus is compute assuming constant volume in the case of a fast process. If this is the case, the radius of meniscus curvature decreases to keep the volume constant as the tip retracts from the substrate and the water meniscus elongates. Whereas the radius of meniscus curvature remains unchanged due to the stabilized pressure different of a water/ vapor interface in constant pressure case since the procedure is slow enough. In our experimental procedure, the retraction velocity of MEMS plate is less than 1 nm/s,

that is, hundreds of times slower than the experiments keeping the meniscus volume steady. As also shown in Fig. 4.3, the theoretic prediction for constant pressure is magnificently consistent with the experimental result. The reason of constant volume hypothesis case is that there is not enough time for water to evaporate if the stretching process is fast and meniscus cannot reach the thermodynamic equilibrium. Theoretic analysis method has demonstrated rather differently without consideration of a Kelvin radius corresponding to the experimental result. According to the so-called Kelvin radius rk provided by the equation, the water meniscus is supposed to be condensed at 0.7 nm apart in the relative humidity of 50 % at room temperature [18]. But in most practical situations the meniscus is confined at the separation distance further than the predicted Kelvin radius [16, 19, 20]. It is much more complicated to understand the capillary force and the surface tension in nanometric system with the classical approaches. The meniscus curvatures obtained by the surface force apparatus (SFA) experiments agree with theoretical values calculated from the Kelvin equation [21, 22], meanwhile other recent studies on the water capillary bridge in various AFM systems observe it in orders of magnitude greater than predicted value by the Kelvin equation [23, 24]. The situation has been less satisfactory for water. There might be another possible explanation that the humidity we have in experiments is different locally close to the condensation point and the local humidity could be presumed as more than 95% by back caculation of the Kelvin equation. On this account we take the radius of curvature as a fitting parameter r_m to investigate the capillary force rather r_k expecting

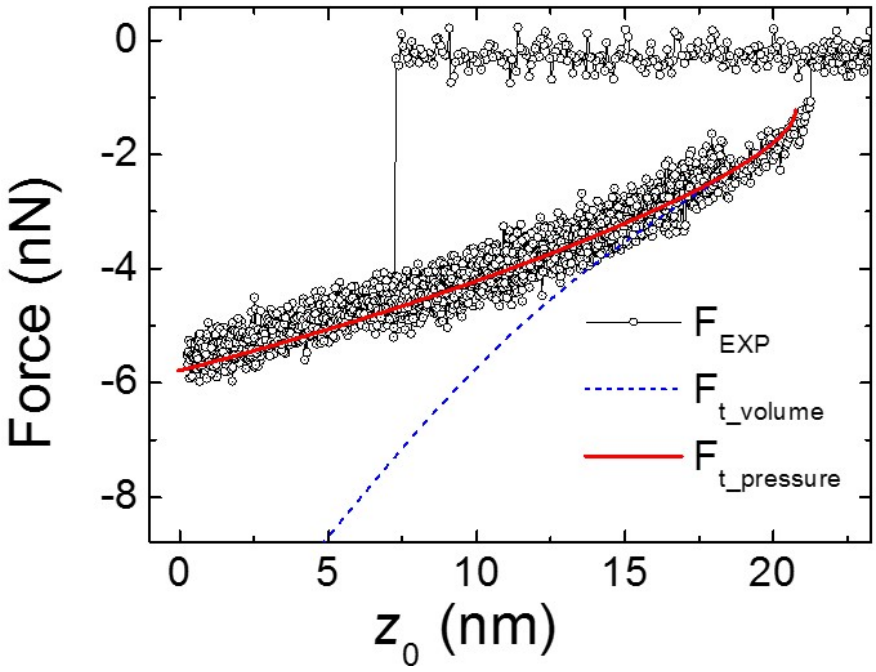

Figure 4.3: Comparison of force distance curve between experimental result from hybrid AFM-MEMS and the theoretical predictions for constant volume and constant pressure, respectively. - The theoretical prediction for constant pressure agrees well with the behavior of the nanometric water meniscus.

from theoretical equation. According to the numerical analysis the force can be calculated with either the tip or the plate and the same result obtained for the total capillary force. The pressure difference of water/ vapor interface is the surface tension divided by the radius of curvature of the nanometric water meniscus. The variables we must consider in accordance with constant pressure hypothesis are the surface tension γ and the radius of meniscus curvature and the numerical solution is formulated in terms of these two variables as follows.

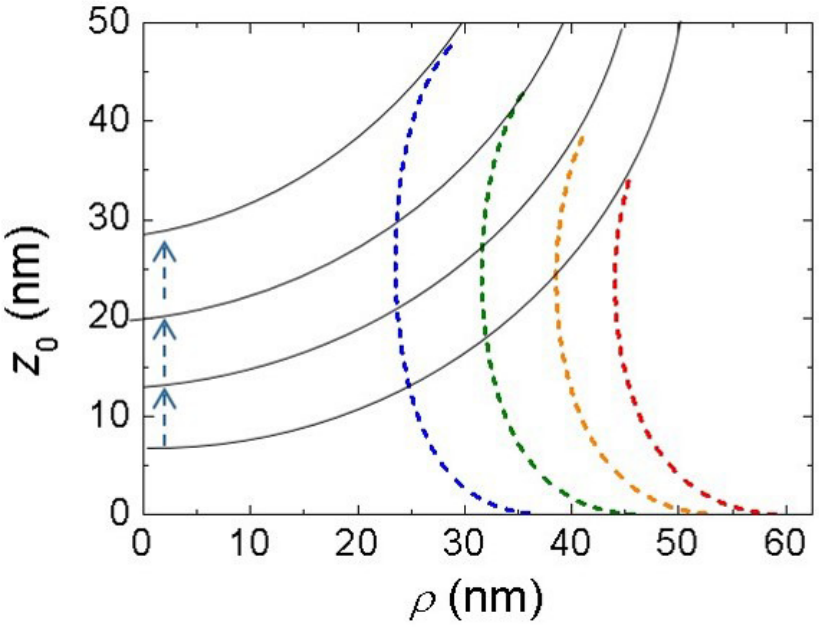

Figure 4.4: Plot of the meniscus curvature r_m, numerically calculated by the Young-Laplace equation, which shows the constant radius of curvature (or equivalently, constant pressure) during meniscus elongation (from red to yellow to green to blue dotted curves) sufficiently slow enough to allow thermal equilibrium with the gaseous environment.

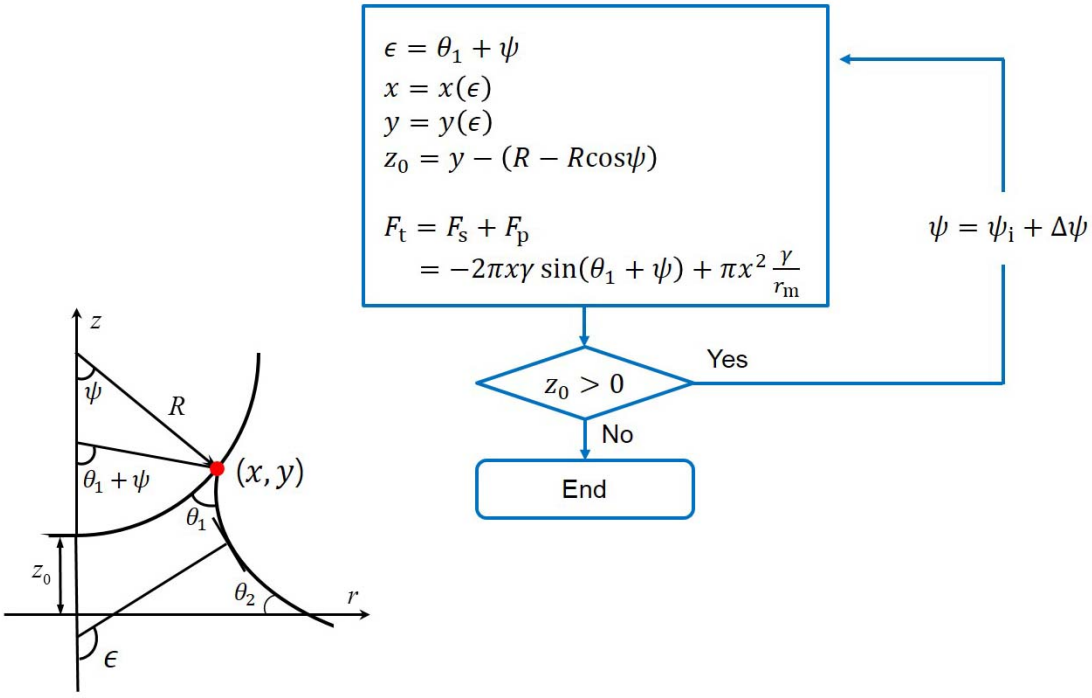

Figure 4.5: Numerical solution of capillary force. The force is computed for all the filling angles ψ during the entire retraction (z_0 ¿0), where the distance z_0 can be evaluated by numerical solution of the Young-Laplace equation for a given ψ.

4.2.4 Theoretic analysis and numerical simulation

Figure S1 presents total/ dimensionless capillary adhesion force simulation for a spherical AFM tip and the flat surface of MEMS calculated under the assumption of constant pressure by use of Eq. 1 in the manuscript. The numerical computation consisted in calculating a solution for all filling angle in a region z_0 ¿ 0 and a contact angle of zero was used in both cases. The study of the

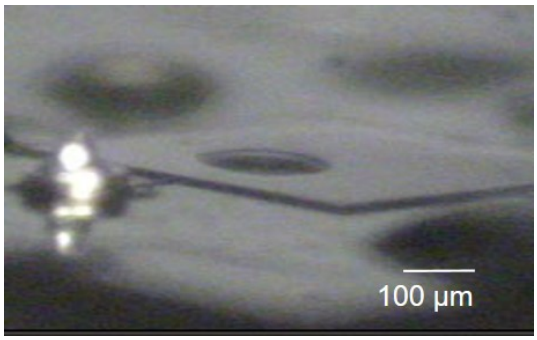

Figure 4.6: The image of the water droplets wetted to the MEMS substrate. For our experiments the silica surface have a contact angle of 11.6° around 150μm.

contact angle dependence experiment on the water droplet line curvature and calculating values of the line tension of a solid-liquid-vapor phase system investigates the silicon dioxide surface in micrometer scale has the negative three phase line tension of about -10^{-9}J/m. The experiments and calculation of a size-dependent variation of the contact angle suggest [25,26] that we reaches the contact angle of zero with the radius of meniscus curvature below 118 nanometer based on the water droplets wetted to the MEMS surface as shown in Fig. 4.6.

Figure 4.7 a indicates that the rupture distance increases along with radius of meniscus curvature and the shape of force-distance curve changes. The magnitude of capillary force increase proportionally to the surface tension while the rupture distance z_r and the force shape maintain the same as shown in Fig. 4.7 c. Dashed line in each plots indicates a physically meaningless solution.

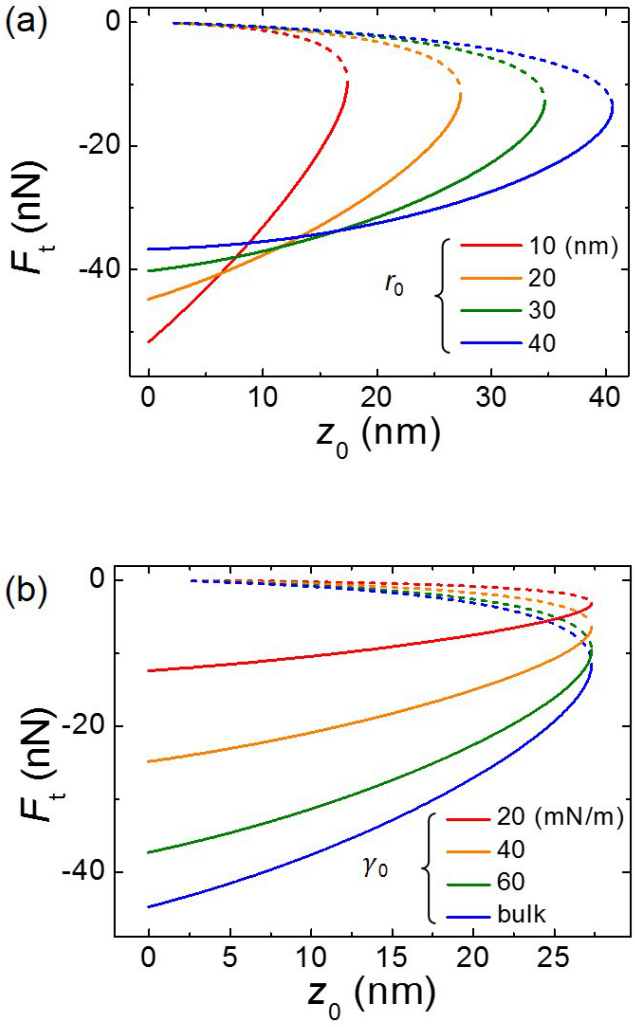

Figure 4.7: Simulation set of Young-Laplace equation for various radius of meniscus curvature and surface tension values, respectively. Total capillary force depending on (a) radius of meniscus curvature rm and (b) surface tension γ as a function of separation distance, calculated by numerical solution of the Young-Laplace equation. The numerical simulation was performed with the value of 50 nm for the AFM tip radius of curvature R and 71.97 mN/m for the surface tension of the bulk water at room temperature corresponding to experimental conditions. Dashed line in plot represents a physically meaningless solution.

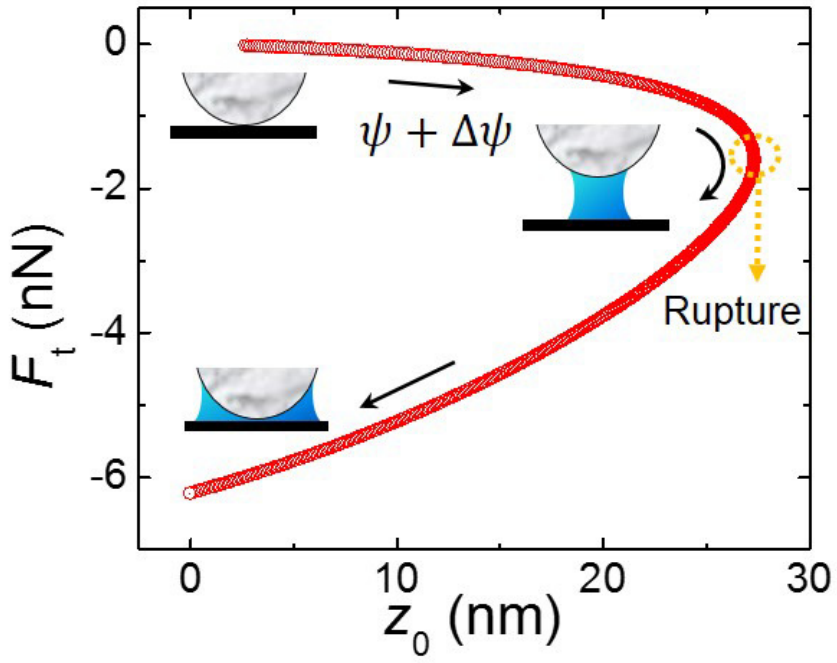

Figure 4.8: Fitting Method using Young-Laplace equation. A typical calculation result of the total capillary adhesion force F_t under the assumption of constant curvature, which can be used to determine the unique best-fitting surface tension value of the water nano-meniscus, γ_m, as well as its corresponding radius of curvature, r_m. The force is computed for all the filling angles ψ during the entire retraction, where the distance z_0 can be evaluated by numerical solution of the Young-Laplace equation for a given ψ. The numerical solution does not exist for distance z_0 beyond z_r where no water meniscus satisfying the Young-Laplace equation exists and z_r corresponds to the rupture point in experiments.

4.2.5 Fitting Method using Young-Laplace equation

The figure 4.8 explains how the experimental results have compared with theoretical calculation. The numerical solution of the capillary force using Young-Laplace equation is for surface tension parameter γ_0 of 10 and the radius of curvature of 20 in Fig. 4.8. The numerical solution does not exist for distance z_0 beyond z_r where no water meniscus satisfying the Young-Laplace equation exists and z_r corresponds to the rupture point of the nanoscale water cluster in experiments. The reason why I only take the specific part of capillary force into account to fit the experimental result is that the solution from the initial value corresponding to ψ minimum to the rupture point (turning point in the calculated capillary force-distance curve) is physically meaningless. For a given ψ, the corresponding values of z_0 is obtained by numerical solution of the Young-Laplace equation with each total capillary force F_{tot} and as a result each distance point z_0 except for the rupture point has two corresponding force values. The solution prior to the rupture point violate the fact that a decrease of the tip-sample distance causes a decrease of the activation energy barrier that leads to a bigger water meniscus [6–8, 27]. There were no reports of such a case in nature that the capillary condensed water meniscus becomes smaller when the tip approaches to the substrate.

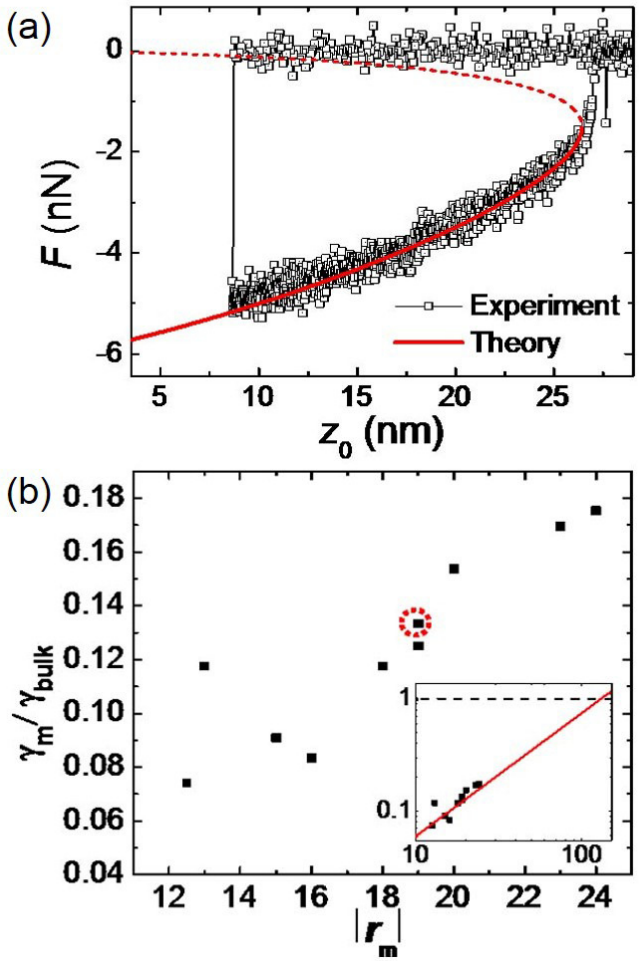

Figure 4.9: Comparison between an experimental force curves and the corresponding to theoretic force distance curves. (a) The curve represents the calculated values by numerical solution of Young-Laplace equation and it shows excellent agreement with experimental data. (b) The surface tension ratio ($\gamma_m/\gamma_{\text{bulk}}$, where γ_{bulk} is a surface tension of bulk water at room temperature, 71.97mN/m) in various radius of meniscus curvature r_m. Each data point here is obtained by individual experiment and theoretical fitting and red dash circle corresponding result from Fig 4.7(a) experiment. Notice that the simple linear extrapolation of the data shown in the inset expects the bulk-value behaviour of surface tension above r_m 130 nm.

4.3 Investigation of surface tension in nanoscale

As a consequence, we obtained smaller surface tension values and decrease along with meniscus curvature. Figure 4.9 b shows obtained surface tension values under 20 % of macroscopically measured surface tension in a region below 25 nm meniscus curvature, and as we simply linear-fit the data points, it seems to reach the surface tension value of bulk liquid water where the meniscus curvature is about 130 nm and appeal to be appropriated by the theory [28]. A negative pressure for bubble formation has about a 0.16 times smaller value in experiments [5] than theoretic prediction by nucleation rate theory for vapor [3] and the discrepancy can be clarified with a reduced surface tension value under 30 % [Appendix]. The surface tension would have to be reduced to 30 % of macroscopic value by the approach of cluster model for bubble formation as well [29–31]. The smaller surface tension in nanoscale allows a possible explanation for energy barrier disagreement [6–8]. We also carried out molecular dynamics simulation about nano curvature system with nano droplet and nano bubble. For nano droplet simulation, we initially put water cluster with cubic shape in the center of the simulation cell. During calculation, cubic water cluster transforms its shape to the spherical, minimizing its surface energy. We used system containing by 181, 511, 2180 water molecule, corresponding radius of nano droplet $R_{droplet}$ = 1nm, 1.45nm, 2.4nm, respectively. Nano bubble was prepared with adopted method shown in Ref [32]. Initially, simulation cell was fully filled with density = 940g/cm^3. After equilibriation, water cluster having

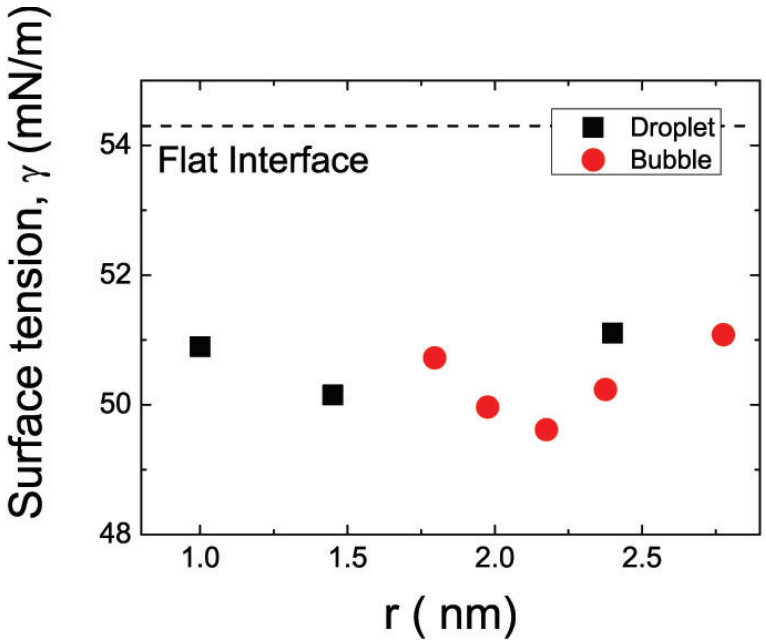

Figure 4.10: Molecular dynamics simulation results of nano curvature system. Both droplet and bubble shows a decrease in surface tension value where the radius of curvature is a couple of nanometer scale.

radius R_{init} was deleted manually to make spherical cavity. During calculation, initial cavity size changes and stabilized nano bubble is formed with R_{bubble}. We calculated five nano bubble simulation with R_{bubble} = 1.79, 1.975, 2.176, 2.375, 2.777nm. All simulation was carried on GROMACS 4.5.5 package [33]. The result shows that the surface tension decrease in nano curved system qualitatively supported by MD simulation.

On this wise, these observations provides a prominent result to understand the properties of water in capillary meniscus better and it may even contribute to practical applications where the confined system being exposed to air plays an important role. Especially, in nanoscale, water capillaries play a

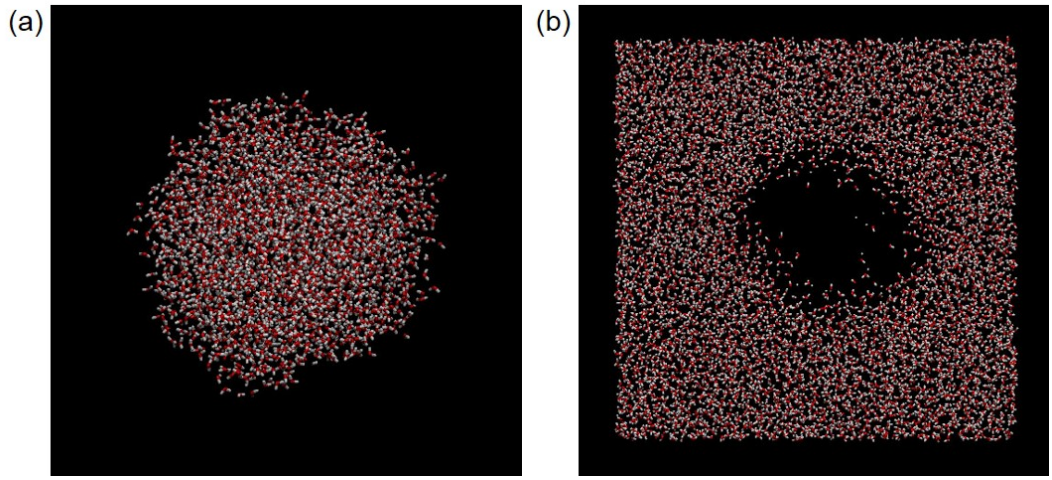

Figure 4.11: Molecular dynamics simulation results of nano curvature system. Both droplet and bubble shows a decrease in surface tension value where the radius of curvature is a couple of nanometer scale.

crucial key for investigation of the particle interaction process in air and self-assembly of bio-molecules and the study of capillary force of the nanometric water meniscus allows valuable understandings of the surface science [34–36].

4.4 Conclusion

The values of the surface tension are derived by direct comparison of the measured interaction forces and the numerical simulations based on the Young-Laplace equation. Here we observed the decrease of the surface tension to 25-nm radius of curvature for which the meniscus has surface tensino about 20% of the bulk value, and show how the results provide a possible resolution of the afore-mentioned discrepancies.

In conclusion, we have quantified the curvature-dependent surface tension

at the nanoscale by measurement of the total capillary force resulting from the water nano-meniscus in combination with theoretical calculation of the r_m.

Bibliography

[1] R. Zhang, A. Khalizov, L. Wang, M. Hu and W. Xu, Chem. Rev. **112**, 1957 (2012).

[2] P. E. Wagner and R. Strey, J. Chem. Phys. **80**, 5266 (1984).

[3] J. C. Fisher, J. Appl. Phys. **19**, 1062 (1948).

[4] H. N. V. Temperley, Proc. Phys. Soc. **59**, 199 (1947).

[5] L. J. Briggs, J. Appl. Phys. **21**, 721 (1950)

[6] B. Sung, J. Kim, C. Stambaugh, S. Chang and W. Jhe, Appl. Phys. Letts. **103**, 213107 (2013).

[7] W. Bak, B. Sung, J. Kim, S. Kwon, B. Kim and W. Jhe, Appl. Phys. Letts. **106**, 013102 (2015).

[8] Y. Men, X. Zhang and W. Wang, J. Chem. Phys. **131**, 184702 (2009).

[9] R. C. Tolman, J. Chem. Phys. **16**, 758 (1948).

[10] H. Y. Kwak and S. D. Oh, J. Colloid. Interf. Sci. **278**, 436 (2004).

[11] L. R. Fisher and J. N. Israelachvili, Chem. Phys. Lett. **76**, 325 (1980).

[12] M. P. Moody and P. Attard, Phys. Rev. Lett.**91**, 056104 (2003).

[13] A. Laaksonen, V. Talanquer D. W. Oxtoby, Annual Reviews, Inc. **46**, 489 (1995).

[14] B. J. Block, S. K. Das, M. Oettel, P. Virnau1 and K. Binder, J. Chem. Phys. **133**, 154702 (2010).

[15] S. Kwon, C. Stambaugh, B. Kim, S. An and W. Jhe, Nanoscale **6**,5474 (2014).

[16] M. Lee, B. Sung, N. Hashemi and W. Jhe, Faraday Discuss. **141**, 415 (2009).

[17] F. M. Orr, J. Fluid Mech. **67**, 723 (1975).

[18] Israelachvili, J. Intermolecular and Surface Forces. Academic Press, New York (2011)

[19] B. Kim, Q. Kim, S. Kwon, S. An, K. Lee and W. Jhe, Phys. Rev. Lett. **111**, 246102 (2013).

[20] S. An, C. Stambaugh, G. Kim, M. Lee, Y. Kim, K. Lee and W. Jhe, Nanoscale **4**, 6493 (2012).

[21] M. M. Kohonen, H. K. Christenson, Langmuir **16**, 7285 (2000).

[22] L. R. Fisher, R. A. Gamble, J. J. Middlehurst, Nature **290**, 575 (1981)

[23] Joost W. van Honschoten, Nataliya Brunets, Niels R. Tas. Chemical Society Reviews **39**, 1096 (2010).

[24] Brandon L. Weeks, Mark W. Vaughn, James J. DeYoreo. Langmuir **21**, 8096 (2005).

[25] J. K. Berg, C. M. Weber and H. Riegler, Phys. Rev. Lett. **105**, 076103 (2010).

[26] D. Aronov, G. Rosenman and Z. Barkay, J. Appl. Phys. **101**, 084901 (2007).

[27] E. Sahagun, P. Garcia-Mochales, G. M. Sacha and J. J. Saenz, Phys. Rev. Lett. **98**, 176106 (2007).

[28] E. A. Guggenheim, Trans. Faraday Soc. **35**, 397 (1940).

[29] G. E. Walrafen, J. Chem. Phys. **44**, 1546 (1966).

[30] F. M. Fowkes, Ind. Eng. Chem. Res. **56**, 40 (1964).

[31] H. Y. Kwak and R. L. Panton, J. Chem, Phys. **78**, 5795 (1983).

[32] M. Matsumoto, J. Fluid Sci. Tech. **3**, 922-929 (2008).

[33] B. Hess, C. Kutzner, D. van der Spoel, and E. Lindahl, J Chem Theory Comput **4**, 435–447 (2008).

[34] M. Nosonovsky and B. Bhushan, Phys. Chem. Chem. Phys. **10**,2137 (2008).

[35] H. J. Butt and M. Kappl, Adv. Colloid Interface Sci. **146**, 48 (2009).

[36] P. J. Yunker, T. Still, M. A. Lohr and A. G. Yodh, Nature **476**, 308 (2011).

Chapter 5

Conclusions

Surface tension is one of ubiquitous physical quantities that play a critical role in wide areas of science and engineering, ranging from nucleation of nano-bubbles to stabilization of proteins to controlled surface accumulation of compounds especially for water. Despite extensive theoretical studies on the surface tension for decades, however, it has been very difficult to quantify, and there are still on-going debates on the validity of bulk surface tension value for nanoscale water. There have been noticeable discrepancies between experimental results and theoretical predictions for the liquid-vapour phase-transition processes, which remains unresolved and yet to be established experimentally. Therefore, a well-controlled experiment that quantifies unambiguously surface tension value in nanoscale is in high demand, where the full-range and accurate force measurement can be made. For this purpose, the nanometric water meniscus best fits due to its uniquely proven stability, controllability and force-sensitivity.

We accomplished absolute capillary force measurement and theoretical analysis of the nanometric water meniscus condensed between an AFM tip and a MEMS surface under ambient condition. Such a nanoscale meniscus is ubiquitous but still poorly understood how the meniscus structure varies and it behaves differently to macroscale. We obtained the full capillary force profile of water bridge by means of a versatile MEMS-AFM system and computed Young-Laplace equation to interpret experimental finding. In our hybrid system, the QTF-based AFM detects the dynamic force gradient that provides information on the viscoelasticity of the meniscus, while the MEMS sensor obtains the absolute static capillary force in full range. The results presented here show an excellent agreement in capillary force. Besides the hybrid MEMS-AFM system with dual capability of stress-strain measurement allows to reveal the unique viscoelastic properties of nanometric water meniscus by obtaining the Young's modulus as well as time-lag response.

The analytical method is applied to determine the surface tension in nanometric water meniscus based on Young-Laplace equation and the numerical computation results are compared to experimental capillary force of the nanometric water bridge investigated by means of the hybrid MEMS-AFM. Based on these experimental observations, the investigation reveals that the surface tension in nanoscale have a value of 20% of the one in bulk water. The value of surface tension reaches a seventh of the one in bulk water, although the radius of surface curvature of capillary water bridge is dozens of times bigger in size than water molecule. This can also indicate that the structure of the meniscus

surface for small systems is not the same as the one in macroscale.

These observations provides a prominent result to understand the surface tension of nanometric water meniscus better and it may even contribute to resolve the existing discrepancies between experiments and theories related to phase transition effects in nanoscale. Nevertheless, the studies in the dissertation could extend the understanding of the microscopic surface tension in various nanoscale structures as well as practical applications such as self-assembly of bio-molecules and nano-bio-materials.

Appendices

Appendix A

Nano-bubble formation and surface tension

A.1 The predicted surface tension by nucleation theory

The theory of nucleation states the rate (J) of formation of bubbles of vapor [1]

$$J = \frac{NkT}{h}\exp\left[-(\Delta {f_0}^* + \frac{16\pi\gamma^3}{3p^2}/kT\right], \tag{A.1}$$

where $\Delta {f_0}^*$ is the free energy of activation, p the pressure, γ surface tension at given temperature T, pressure p. The rate of bubble formation derived from the net work associated with the formation of a sperical vapor bubble which is

presented as,

$$\begin{aligned} W &= \gamma A + pV + p_r V \\ &= 4\pi r^2\gamma + \frac{4}{3}\pi r^3(p - p_r) \\ &\simeq 4\pi r^2\gamma + \frac{4}{3}\pi r^3 p \end{aligned} \tag{A.2}$$

The work pV is contributed by the formation of a cavity of volume V when liquid is under negative pressure p, γA by formation of the liquid-vapor interface bounding the bubble and $-p_r V$ to fill the bubble reversibly with vapor of pressure p_r. When the p_r is negligible in comparison with p, the net work can be simplified as above and it has a maximum value of $16\pi\gamma^3/3p^2$ for a bubble radius of $r^* = -2\gamma/p$.

The first bubble that forms fractures the liquid water gives the negative pressure (assuming ${\Delta f_0}^*$ is zero corresponded to minimum p),

$$p_t = -\left[\frac{16\pi}{3}\frac{\gamma^3}{kT\ln NkT/h}\right]^{1/2} \tag{A.3}$$

The calculated pressures (1778 atm) are about 6 times bigger than the experimental values (277 atm) [2] and for these results to agree satisfactorily one might think that the surface tension should be required rather smaller than macroscopic surface tension. If we assume the nanoscopic surface tension is different and numerically 30 % of the macroscopic value ($\gamma \propto p^{2/3}$), the pressure obtained by the nucleation theory have the same result from experiments.

A.2 The cluster model for bubble formation

The cluster model for bubble formation suggests the surface tension as follows [3],

$$\gamma = \frac{r_0}{2}\left(\frac{12\epsilon}{3\nu_0}\right) \tag{A.4}$$

Here r_0 is the radius of a liquid water molecule, ν_0 the effective molecular volume of the liquid, ϵ the energy to separate a pair of molecules from a distance d_0 apart to the distance d_c (mean distance between molecules at the critical point) [4]

$$\epsilon = -4\epsilon_0\left[1-\left(\frac{\rho_c}{\rho_0}\right)\right]\left[\left(\frac{d}{d_0}\right)^6-\left(\frac{d}{d_0}\right)^{12}\right] \tag{A.5}$$

with $\epsilon_0 = \frac{3E_I\alpha^2}{16d^6}$, where ρ_c is the critical density, ρ_0 the liquid density, E_I the ionization potential, α the polarizability of a liquid molecule. The cluster model for bubble formation, therefore, predicts the surface tension value γ as about 22 % of macroscopic surface tension value.

Appendix B

Numerical calculation of capillary force in water nanomeniscus

In this Appendix, we present the details of the numerical calculation of capillary force to obtain the surface tension in nanoscale water meniscus as shown in Chapter 4. We used Mathematica 9.0 for the calculation and the programming is an example to accomplish the numerical simulation in Chapter 4.

```
SetDirectory["C:\\math"];
Vm = 1.8*10^-5 (* molar volume, m^3/mole*);
ga = (1/6)*72*10^-3 (*gamma, surface tension,N/m*);
R0 = 8.31 (*gas constant, J/mole K *);
T = 298 (* temperature, K *);
Rh = 0.95(* relative humidity *);
rm = -23*10^-9 (*radius of meniscus curvature *);
H = 1/(2*rm); (*mean curvature_orr*)
the1 = (Pi/180)*0(* contact angle of tip*);
the2 = (Pi/180)*0 (* contact angle of sample*);
R = 50*10^-9 (*tip radius, m*);
psi = (Pi/180)*2(* filling angle *);
Xi = the1 + psi;
pi = Pi/2 - Xi;
pi1 = -(the1 + psi) + Pi/2;
pi2 = the2 - Pi/2;

u = -Sin[Xi];

c = 4*(H*R*Sin[psi])^2 - 4*R*H*Sin[psi]*Sin[the1 + psi];
k = 1/Sqrt[1 + c];
THETA = -Cos[the1 + psi] - Cos[the2];
mu = (c + 4)*THETA + (4/3)*(Cos[the1 + psi]^3 + Cos[the2]^3);
nu = (4/3)*Sin[the1 + psi]*Cos[the1 + psi]*
    Sqrt[Sin[the1 + psi]^2 + c];
eta = (4/3)*Sin[the2]*Cos[the2]*Sqrt[Sin[the2]^2 + c];
omega = Pi/((2*H*R)^3);
x = (Sin[Xi] - Sqrt[Sin[Xi]^2 + c])/(2*H);
```

```
y =
   1/(2 H) *
    ((-Cos[the2] - Cos[Xi]) -
      1/k * (EllipticE[pi2, k] - EllipticE[pi, k]) +
      (1 - k^2)/k * (EllipticF[pi2, k] - EllipticF[pi, k]));

Vol1 =
  omega *
    (mu + nu + eta - 1/3 * k * c * (c + 4) *
       (EllipticF[pi1, k] - EllipticF[pi2, k]) +
      1/3 * k * (c + 8) * (c + 1) *
       (EllipticE[pi1, k] - EllipticE[pi2, k])) * R^3;
Vol2 = Pi * (2 / 3 - Cos[psi] + (Cos[psi]^3) / 3) * R^3;
Vol = Vol1 - Vol2;
Xi = psi + the1;
zd = y - R * (1 - Cos[psi]);
the1i = the1;
psii = psi;


imax = 1000;
sol = Table[{0, 0, 0, 0, 0, 0, 0, 0, 0, 0, 0}, {i, 1, imax}];

For[i = 1, i < imax + 1 && zd > 0, i++,
  psi = psii + (Pi / 180) * i / 10;
```

```
Xi = the1 + psi;
pi = Pi / 2 - Xi;
pi1 = -(the1 + psi) + Pi / 2;
pi2 = the2 - Pi / 2;

H = 1 / (2 * rm);
c = 4 * (H * R * Sin[psi]) ^ 2 - 4 * R * H * Sin[psi] * Sin[the1 + psi];
k = 1 / Sqrt[1 + c];

THETA = -Cos[the1 + psi] - Cos[the2];
mu = (c + 4) * THETA + (4 / 3) * (Cos[the1 + psi] ^ 3 + Cos[the2] ^ 3);
nu = (4 / 3) * Sin[the1 + psi] * Cos[the1 + psi] *
   Sqrt[Sin[the1 + psi] ^ 2 + c];
eta = (4 / 3) * Sin[the2] * Cos[the2] * Sqrt[Sin[the2] ^ 2 + c];
omega = Pi / ((2 * H * R) ^ 3);

x = (Sin[Xi] - Sqrt[Sin[Xi] ^ 2 + c]) / (2 * H);
y =
  1/(2 H) *
   ((-Cos[the2] - Cos[Xi]) -
     1/k * (EllipticE[pi2, k] - EllipticE[pi, k]) +
     (1 - k ^ 2)/k * (EllipticF[pi2, k] - EllipticF[pi, k]));
```

```
Vol1 =
 omega *
  (mu + nu + eta - 1/3 * k * c * (c + 4) *
     (EllipticF[pi1, k] - EllipticF[pi2, k]) +
    1/3 * k * (c + 8) * (c + 1) *
     (EllipticE[pi1, k] - EllipticE[pi2, k])) * R^3;;
Vol2 = Pi * (2 / 3 - Cos[psi] + (Cos[psi]^3) / 3) * R^3;
Voln = Vol1 - Vol2;

u1 = -Sin[psi + the1];
u2 = -Sin[Pi - the1];
Ft = -2 * Pi * x * ga * Sin[psi + the1];
Fp = Pi * x^2 * ga / rm;
Fc = Ft + Fp;
zd = y - R * (1 - Cos[psi]);
Xi = Pi - the2;
x = (Sin[Xi] - Sqrt[Sin[Xi]^2 + c]) / (2 * H);
Ftsurf = -2 * Pi * x * ga * Sin[Pi - the2];
Fpsurf = Pi * x^2 * ga / rm;
Fcsurf = Ftsurf + Fpsurf;
Forr =
 2 * Pi * R * ga
  (-Sin[psi] * Sin[the1 + psi] + (R * (Sin[psi])^2) / (2 * rm));
```

```
  sol[[i, 1]] = N[Re[zd] * 10^9];
  sol[[i, 2]] = N[Forr];
  sol[[i, 3]] = N[Ft];
  sol[[i, 4]] = N[Fp];
  sol[[i, 5]] = N[Fc];
  sol[[i, 6]] = N[Ftsurf];
  sol[[i, 7]] = N[Fpsurf];
  sol[[i, 8]] = N[Fcsurf];
  sol[[i, 9]] = N[Voln];
  sol[[i, 10]] = N[180 * psi / Pi];
  sol[[i, 11]] = N[rm];
  Print[{N[i], N[rm], N[zd]}];
 ];

Export["check_Orr_nc_rm23_r50_g6.dat", sol]
```

Appendix C

Fabricated tips for hybrid MEMS-AFM system

C.1 Quartz tip fabricated by a laser puller

We fabricated the quartz tip using a commercial laser puller (P-2000, Sutter Instruments Co.) to produce the rigid tip with a various radii. At any cases, quartz is oxidized silicon while Si is single crystal. When we place Si tips in our setup, the outer layer of Si tip turns to silicon oxide. The compound is harder than pure substance, but it actually breaks easier since only a few outer layers changed. As shown in Fig. C.1 (b) the Si cantilver tip changes its radius and shape quite a lot after the experiments when it experience contacts with substrate. While quartz is already oxidized form of Si, so it is not happening like Si. From material difference, it can cause the difference in our experiment

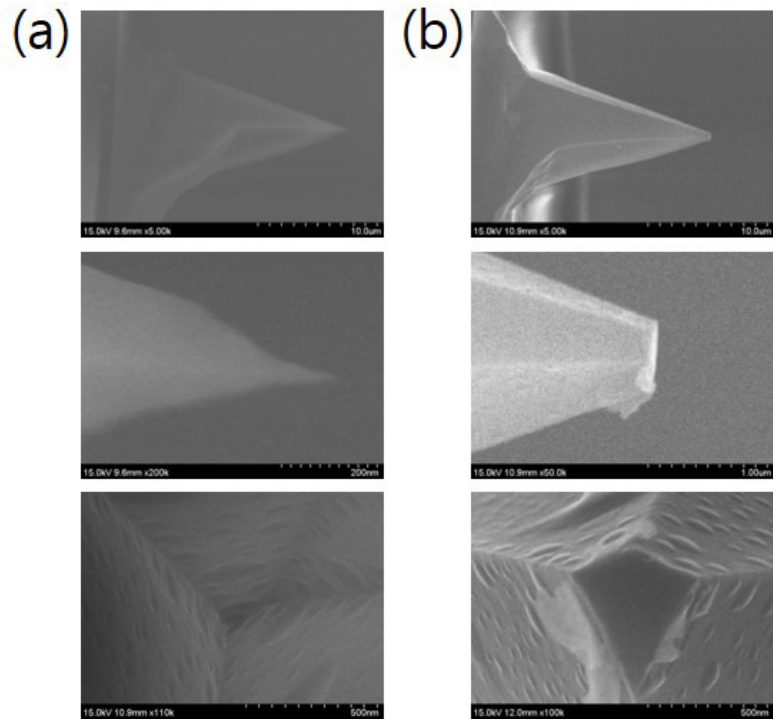

Figure C.1: SEM images of a silicon cantilever tip. (a) The fresh cantilever tip before experiments. (b) Tips have been used for experiments after the contact with the substrate. The Si tip has undergone great changes in its shape and radius which changed from 10 nm up to 2∼300 nm in a contact experiment.

advantages besides the shape changes less in quartz tips. Figure C.2 presents the radius of the fabricated quartz tip changes as we do experiment on contact. The radius of fabricated quartz tip changes from 13nm to 50nm while the Si cantilver tip has undergone great changes in its shape and radius which changed from 10 nm up to 2∼300 nm in a contact experiment.

By changing variables in the commercial laser puller, we can make a variety of sizes.

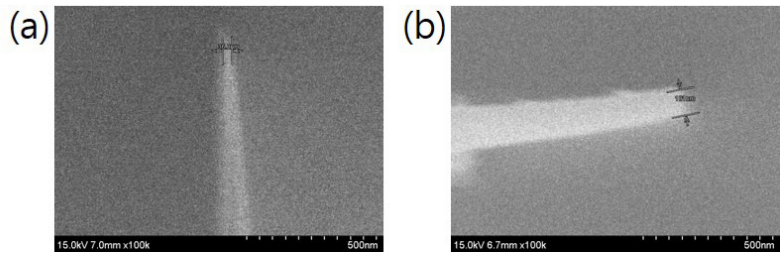

Figure C.2: SEM images of a fabricated quartz tip. (a) The fresh quartz tip before experiments. (b) Fused quartz tip for experiments after the contact with the substrate.

C.2 The size control capability

Figure C.3 shows a procedure of pulling quartz rod in order to fabricate size-controlled rigid tips for experiments. The tip diameter can be determined by mostly delay and pull values (Tip diameter = $\frac{\text{delay}}{\text{pull}}$).

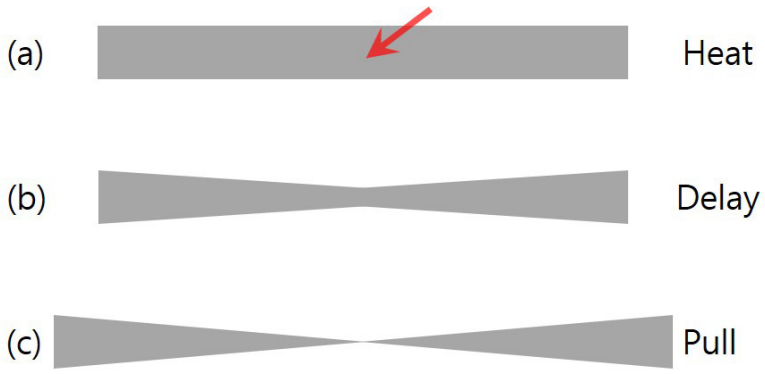

Figure C.3: The size control capability in fabrication with variables. (a) Heat value control the output power of laser which can melt the quartz rod in the middle. (b) Increasing the delay results in decreased taper length and increased tip diameter. (c) The higher the pull, the smaller the tip diameter, the longer the taper as well.

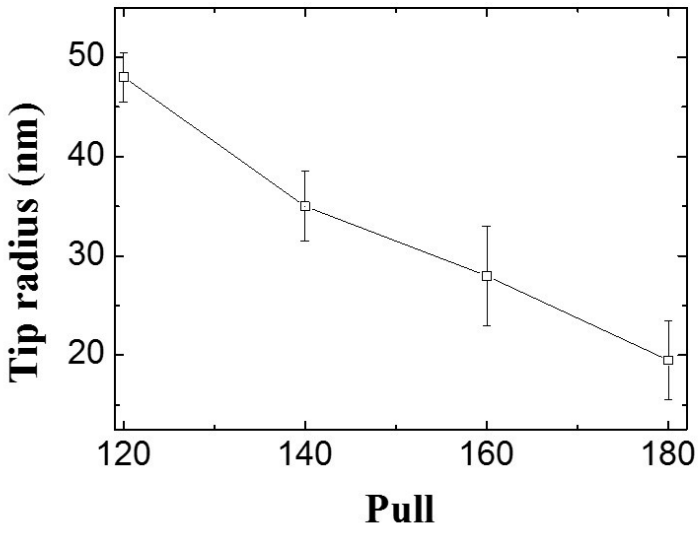

Figure C.4: A variety of sized-tip fabricated depeding on pull values of the laser puller

Bibliography

[1] J. C. Fisher, J. Appl. Phys. **19**, 1062 (1948).

[2] L. J. Briggs, J. Appl. Phys. **21**, 721 (1950)

[3] H. Y. Kwak and S. D. Oh, J. Colloid and Interface Sci. **278**, 436 (2004)

[4] H. Y. Kwak and R. L. Panton, J. Phys. D: Appl. Phys.**18**, 647 (1985)

초 록

표면장력은 나노 물 매니스커스나 기포의 응축, 증발 등 나노미터 크기에서의 기체-액체 상전환에 중요한 역할을 한다. 나노사이즈 물 기둥이나 기포가 형성에 있어 실험적으로 측정된 값과 이론값이 큰 차이를 보여왔으며, 이는 거시적인 크기에서의 표면장력 값이 나노스케일에서도 같을 것인지에 대해 논란이 제기되어 왔다. 하지만 아직 표면장력값은 잘 밝혀지지 않은채 남아있고 더 나은 이해가 반드시 필요하다. 표면장력을 측정하는 방법에는 여러가지가 있으나 모세관을 이용한 방법은 표면장력을 결정하는데 가장 오래되고 대표적인 방법이다. 우리는 하이브리드 힘 측정장치를 고안하여 실험적으로 어려웠던 나노스케일에서의 모세관힘을 측정하고 표면장력을 연구하였다.

수정진동자를 기반한 진폭 변조 원자힘현미경을 미소 전자 기계 시스템과 결합한 하이브리드 시스템은 친수성 표면 사이에 나노사이즈의 공간에 가둬진 물기의 동적, 정적인 힘을 측정하였다. 이 시스템은 안정적인 두께의 나노스케일 물기둥을둥 형성하고 정확한 모세관힘 측정과 동시에 나노 물 매니스커스의 동역학적 특성을 분석하였다. 응력과 변형 실험을 통해 나노 물 매니스커스가 부드러운 고무나 세포조직과 비슷한 탄성율을 가지고 있음을 알았으며, 손실탄젠트를 얻어 고체유사상태에 가까운 점탄성 물질임을 정확히 분석해냈다. 그리고 실험결과를 영-라플라스 방정식에 기반하여 계산한 값과 비교하였고 이 수치평가를 통해 나노스케일에서 조금 더 면밀한 표면장력 연구가 가능하게 되었다. 그리하여 나노스케일에서 물 매니스커스의 표면장력 값이 거시계에서 물의 표면장력의 20% 이하로 크게 줄어든다는 것을 알게 되었다.

이러한 표면장력의 연구는 액체-기체 상전환 효과와 연관되어 실험과 이론 사이에 존재해왔던 불일치를 해결 할 실마리를 제시해 줄 수 있을 것으로 기대되며, 생체 분자의 자가조립이나 나노물질의 효과적인 설계 등의 응용분야에 기여할 것이다.

주요어 : 나노물, 표면장력, 모세관힘, 미소전자기계시스템, 원자힘현미경

학 번 : 2010-30114